

AD-A100 274

AD

MEMORANDUM REPORT ARBRL-MR-03090

TECHNICAL  
FREE FLIGHT RANGE TESTS OF THE LIBRARY  
COPPERHEAD PROJECTILE

Robert L. McCoy

March 1981



US ARMY ARMAMENT RESEARCH AND DEVELOPMENT COMMAND  
BALLISTIC RESEARCH LABORATORY  
ABERDEEN PROVING GROUND, MARYLAND

Approved for public release; distribution unlimited.

DTIC QUALITY INSPECTED 3

Destroy this report when it is no longer needed.  
Do not return it to the originator.

Secondary distribution of this report by originating  
or sponsoring activity is prohibited.

Additional copies of this report may be obtained  
from the National Technical Information Service,  
U.S. Department of Commerce, Springfield, Virginia  
22161.

The findings in this report are not to be construed as  
an official Department of the Army position, unless  
so designated by other authorized documents.

*The use of trade names or manufacturers' names in this report  
does not constitute endorsement of any commercial product.*

~~UNCLASSIFIED~~

SECURITY CLASSIFICATION OF THIS PAGE (When Data Entered)

UNCLASSIFIED

SECURITY CLASSIFICATION OF THIS PAGE(*When Data Entered*)

tests are too sparse to permit a quantitative determination of limit-cycle behavior.

UNCLASSIFIED

SECURITY CLASSIFICATION OF THIS PAGE(*When Data Entered*)

TABLE OF CONTENTS

	Page
LIST OF ILLUSTRATIONS . . . . .	5
LIST OF TABLES . . . . .	7
I. INTRODUCTION . . . . .	9
II. TEST MATERIAL AND PROCEDURE . . . . .	10
III. RESULTS . . . . .	11
A. Drag Coefficient . . . . .	12
B. Pitching Moment, Normal Force, and Center of Pressure . . . . .	13
C. Magnus Moment Coefficient and Pitch Damping Moment Coefficient . . . . .	14
D. Damping Rates . . . . .	15
IV. CONCLUSIONS . . . . .	15
REFERENCES . . . . .	51
APPENDIX . . . . .	53
LIST OF SYMBOLS . . . . .	61
DISTRIBUTION LIST . . . . .	63

LIST OF ILLUSTRATIONS

Figure	Page
1. Sketch of the XM712 Projectile . . . . .	17
2. Photograph of XM712 Projectiles . . . . .	18
3. Shadowgraph of B0 35 Model at Mach 1.78 . . . . .	19
4. Shadowgraph of B0 35 MOD Model at Mach 1.48 . . . . .	20
5. Shadowgraph of B0 40 Model at Mach 1.49 . . . . .	21
6. Shadowgraph of B0 35 Model at Mach 1.20 . . . . .	22
7. Shadowgraph of B0 35 MOD Model at Mach 1.19 . . . . .	23
8. Shadowgraph of B0 40 Model at Mach 1.20 . . . . .	24
9. Shadowgraph of B0 35 Model at Mach 1.04 . . . . .	25
10. Shadowgraph of B0 35 MOD Model at Mach 1.02 . . . . .	26
11. Shadowgraph of B0 40 Model at Mach 1.01 . . . . .	27
12. Shadowgraph of B0 35 Model at Mach 0.98 . . . . .	28
13. Shadowgraph of B0 35 MOD Model at Mach 0.97 . . . . .	29
14. Shadowgraph of B0 40 Model at Mach 0.98 . . . . .	30
15. Shadowgraph of B0 35 Model at Mach 0.81 . . . . .	31
16. Shadowgraph of B0 35 MOD Model at Mach 0.80 . . . . .	32
17. Shadowgraph of B0 40 Model at Mach 0.81 . . . . .	33
18. Zero-Yaw Drag Force Coefficient versus Mach Number . . . . .	34
19. Quadratic Yaw Drag Force Coefficient versus Mach Number . . . . .	35
20. Zero-Yaw Pitching Moment Coefficient versus Mach Number . . . . .	36
21. Cubic Pitching Moment Coefficient versus Mach Number . . . . .	37

LIST OF ILLUSTRATIONS

Figure	Page
22. Quintic Pitching Moment Coefficient versus Mach Number . . . . .	38
23. Zero-Yaw Normal Force Coefficient versus Mach Number . . . . .	39
24. Cubic Normal Force Coefficient versus Mach Number . . . . .	40
25. Quintic Normal Force Coefficient versus Mach Number . . . . .	41
26. Zero-Yaw Center of Pressure versus Mach Number . . . . .	42
27. Magnus Moment Coefficient versus Mach Number . . . . .	43
28. Pitch Damping Moment Coefficient versus Mach Number . . . . .	44
29. Fast Arm Damping Rate versus Mach Number . . . . .	45
30. Slow Arm Damping Rate versus Mach Number . . . . .	46
A-1. Smear Camera Photograph of B0 35 MOD Model with Broken Nose Cap, Round No. 16520 . . . . .	54
A-2. Pitch-Plane Shadowgraph of Round No. 16520, Station 11 . . . . .	55
A-3. Pitch-Plane Shadowgraph of Round No. 16520, Station 14 . . . . .	56
A-4. Pitch Plane Shadowgraph of Round No. 16520, Station 15 . . . . .	57
A-5. Pitch Plane Shadowgraph of Round No. 16520, Station 24 . . . . .	58
A-6. Pitch Plane Shadowgraph of Round No. 16520, Station 25 . . . . .	59

LIST OF TABLES

<u>Table</u>		<u>Page</u>
I.	Physical Characteristics. . . . .	47
II.	Summary of Aerodynamic Characteristics . . . . .	48
III.	Summary of Flight Motion Characteristics . . . . .	50

## I. INTRODUCTION

On 1 August 1978, a Copperhead (XM712) Quarterly Review was held at the Martin Marietta Corporation (MMC) facility in Orlando, Florida. The Aerodynamic Working Group meeting, held in conjunction with the Quarterly Review, was charged by the Project Manager, Cannon Artillery Weapons Systems (PM-CAWS) to address the results of recent XM712 flight tests conducted at White Sands Missile Range (WSMR), and recommend a test plan to investigate the potential problems.

The WSMR flights had been instrumented with on-board accelerometers, and the telemetry data had indicated the existence of "coning motion," or limit-cycle yaw, at transonic speeds. In addition, MMC personnel had analyzed the results of tracking radar data on the same flights, and the radar data showed larger round-to-round variation in total aerodynamic drag than would normally be expected.

The second potential problem centered around the proposed use of "gutted" rounds for Firing Table tests, which were scheduled to be conducted in the near future. Due to the porosity of the XM712 body surface, generated by the requirement for fin and wing slots, and the rather high sensitivity to porosity of aerodynamic drag and lift indicated by wind tunnel tests<sup>1</sup>, the consensus of the Aerodynamic Working Group was that full-scale, free-flight tests should be conducted, to firmly establish the aerodynamic differences between "gutted" and all-up-control-section rounds.

By mid-January 1979, a test plan was finalized between the Ballistic Research Laboratory (BRL), PM-CAWS, and MMC. The plan consisted of a nineteen round firing program in the BRL Transonic Range<sup>2</sup>, to establish the aerodynamic differences between three variations of the XM712 projectile; an all-up-control-section round (B040), a totally "gutted" control-section round (B035), and an "in-between" version (B035-MOD), with closure of sensor holes in the body surface. Funding, authority to conduct the test, and approval of the final test plan were received by BRL in a letter from the PM-CAWS, dated 22 January 1979.

---

1. *W. H. Appich, Jr. and R. E. Wittmeyer, "Copperhead Aerodynamic Test Data, Analyses, and Flight Simulation Model Development, Vol. I and II," Martin Marietta Corporation Report OR 15321, November 1978.*
2. *W. K. Rogers, Jr., "The Transonic Free Flight Range," Ballistic Research Laboratories Report Number 1044, Aberdeen Proving Ground, Maryland, June 1958. AD 200177.*

Projectiles for testing arrived at BRL in early March 1979. Physical measurements were made on a sample of each model type, and firing began on 25 April 1979. Fifteen rounds were successfully launched between 25 April 1979 and 3 May 1979.

On 3 May 1979, the sixteenth round (B035 MOD) in the BRL test program was fired, at a test Mach number of approximately 1.75. A smear camera located roughly 3 metres in front of the gun muzzle showed that the plastic nose-cap had failed, and was disintegrating in flight. The projectile (Test Round No. 16520) pitched upward after entering the range, and continued to climb until it impacted the steel roof trusses of the building, at the end of the third group of stations. The collision resulted in extensive structural and instrumentation damage to the Transonic Range, and forced closure of the range for two months to make necessary repairs.

By mid-July 1979, the Transonic Range was again operational, and the remaining three XM712 projectiles were successfully launched, at a test Mach number of 1.05, on 9-10 August 1979.

The aerodynamic data from the eighteen successful flights have been analyzed, and are presented in this report. Partial data obtained from Round No. 16520 are included in the appendix.

## II. TEST MATERIAL AND PROCEDURE

A total of nineteen rounds were available for the BRL tests, of which six were B040 type, five were B035 type, and eight were B035-MOD projectiles. Physical measurements were made on a sample of three projectiles of each of the three types. Dimensions, weights, and centers of mass were obtained using the methods of Reference 3. The axial and transverse moments of inertia were obtained to within  $\pm 0.03\%$  error, using the Space Electronic Corporation equipment. The average physical characteristics of the test projectiles are listed in Table I. Figure 1 is a sketch of the XM712 projectile, with pertinent external dimensions. Figure 2 is a photograph of one each of the three model types.

The test projectiles were fired from a 155mm, M109A1 Howitzer. Modified charges of M119E4 propellant, Zone-8, were used to launch projectiles at test Mach numbers of 1.5 and up. Lower test Mach numbers

---

3. E. R. Dickinson, "Physical Measurements of Projectiles," Technical Note 874, U. S. Army Ballistic Research Laboratories, Aberdeen Proving Ground, MD, February 1954, AD 803103.

were obtained using modified charges of M4A2 propellant. No attempt was made to induce yaw on any of the first sixteen rounds fired, due to the relatively fragile projectile nose section, and the possibility that some yaw induction techniques might alter the fin deployment rate.

Accurate roll measurements in spark range testing are usually obtained by installing a small roll pin in the outer periphery of the model base. However, MMC personnel advised against such an installation on the Copperhead models, due to a marginal safety factor in allowable stress on the XM712 base section. The method selected for roll measurement was the addition of a "rear latch notch" on the outboard edge of one fin. Unfortunately, the additional notch was often invisible in one or the other plane shadowgraphs, due to the obscuring effect of an adjacent unnotched fin. The result was a reduction in the usually high quality of roll data obtained in the Transonic Range. At least some roll data was obtained on most rounds, however, and is reported as part of the flight motion parameters observed.

### III. RESULTS

The range data were fitted to solutions of the linearized equations of motion and these results used to infer linearized aerodynamic coefficients using the methods of Reference 4. The actual projectile aerodynamic force-moment system often is not strictly linear. Given sufficient data, the actual non-linear behavior also can be determined from free-flight range results<sup>5</sup>. For the present tests, the generally small level of launch yaws, combined with the paucity of data due to the very limited program size, prevented the direct determination of aerodynamic non-linear behavior. However, extensive wind tunnel test results for the Copperhead projectile were available from Reference 1, and the wind tunnel determined non-linear coefficients were used to correct the range values to zero-yaw conditions.

---

4. C. H. Murphy, "Data Reduction for the Free Flight Spark Ranges," Report 900, U. S. Army Ballistic Research Laboratory, Aberdeen Proving Ground, MD, February 1954, AD 35833.
5. C. H. Murphy, "The Measurement of Non-Linear Forces and Moments by Means of Free Flight Tests," Report 974, U. S. Army Ballistic Research Laboratory, Aberdeen Proving Ground, MD, February 1956, AD 93521.

A useful by-product of tests conducted in the BRL aerodynamic ranges is the shadowgraph information obtained. A selected set of comparative shadowgraphs for the three model types at supersonic, transonic, and subsonic speeds are presented in Figures 3 through 17 of this report.

The round-by-round aerodynamic data obtained is listed in Table II. Flight motion parameters, including mid-range roll rate, are given in Table III.

#### A. Drag Coefficient

The drag coefficient,  $C_D$ , is determined by fitting the time-distance measurements from the range flight.  $C_D$  is distinctly non-linear with yaw level, and the value determined from an individual flight reflects both the zero-yaw drag coefficient,  $C_{D_0}$ , and the

induced drag due to the average yaw level of the flight. The drag coefficient variation at small yaw levels is adequately represented by:

$$C_D = C_{D_0} + C_{D_\delta}^2 \delta^2$$

where  $C_{D_0}$  is the zero-yaw drag coefficient,  $C_{D_\delta}^2$  is the quadratic yaw-drag coefficient, and  $\delta^2$  is an average effective squared yaw for the individual flight. The wind tunnel value of  $C_{D_\delta}^2$  from Reference 1 was used to correct the range value of  $C_D$  to zero-yaw conditions.

Figure 18 shows the variation of  $C_{D_0}$  with Mach number for the three model types tested in the Transonic Range. The B040 round has the highest drag coefficient, at all speeds tested; the B035 round has the lowest drag, and the drag of the B035-MOD round is intermediate between the other two types. The drag difference between round types is roughly 2%, for all Mach regions tested. The wind tunnel zero-yaw drag coefficient is plotted as a dashed line on Figure 18 for comparison. The B040 round shows 8% less drag than the wind tunnel values at subsonic speeds; at supersonic speeds the range data are more or less in agreement with the wind tunnel curve.

Figure 19 is a plot of the wind tunnel yaw-drag coefficient,  $C_{D_\delta}^2$ , versus Mach number. The curve of Figure 19 was used to correct the range values of total drag coefficient to the zero-yaw values plotted in Figure 18.

#### B. Pitching Moment, Normal Force, and Center of Pressure

The range values of pitching moment coefficient,  $C_{M_\alpha}$ , were corrected to zero-yaw coefficients,  $C_{M_{\alpha_0}}$ , using the wind tunnel values<sup>1</sup> for the cubic and quintic static moment coefficients. Figure 20 is a plot of the zero-yaw pitching moment coefficient versus Mach number, for the three round types tested in the range. The wind tunnel cubic and quintic pitching moment coefficients are shown in Figures 21 and 22, respectively.

The wind tunnel zero-yaw pitching moment coefficient variation with Mach number is plotted as a dashed curve on Figure 20. The range data show that both the B035 and B035 MOD configurations approach neutral stability at around Mach number 1.5, for small angles of attack. The B040 configuration is more stable at high Mach numbers, and Figure 20 suggests that neutral stability for the B040 model will occur somewhere around Mach number 1.8. Due to the sparsity of data shown in Figure 20, the predicted neutral stability points should be regarded with some skepticism.

Figure 23 shows the variation of the zero-yaw normal force coefficient,  $C_{N_{\alpha_0}}$ , with Mach number. The wind tunnel cubic and quintic normal force coefficient, shown in Figures 24 and 25, respectively, were used to correct the range values of  $C_{N_\alpha}$  to zero-yaw values.

The measurement of normal force (or lift) coefficient is more difficult in free flight range testing than the measurement of pitching moment coefficient, since the normal force is determined from center of mass swerving motion, while the pitching moment is determined directly from the measured epicyclic frequencies. Several of the XM712 rounds launched with extremely small yaw, and insufficient swerving motion was observed for satisfactory determination of  $C_{N_\alpha}$ .

The normal force results shown on Figure 23 are too sparse in number to differentiate between model types, and an average trend curve is shown for supersonic speeds. The only significant conclusion that can be drawn from Figure 23 is that, at supersonic speeds, the range data show roughly 20% less normal force than was determined from wind tunnel testing.

The zero-yaw normal force center of pressure,  $C_{p_{N_0}}$ , is shown in

Figure 26. The range data show variations of up to 1/4 caliber in neutral point location from the wind tunnel curve, but no significant differences among model types are apparent. Figure 26 shows that the neutral point moves forward with increasing supersonic speed, and predicts that the B035 and B035 MOD configurations, with a more aft center of mass location, will approach neutral stability at lower Mach number than will the B040 model, confirming the trend shown in Figure 20.

### C. Magnus Moment Coefficient and Pitch Damping Moment Coefficient

The range values of Magnus moment (Side moment) coefficient,  $C_{M_{pq}}$ , and pitch damping moment sum,  $C_{M_q} + C_{M_\alpha}$ , are plotted in Figures 27 and 28, respectively. No wind tunnel data have been collected for Magnus or pitch damping moments on the XM712 projectile; hence no non-linear effects were available to correct the range values to zero-yaw conditions. An unsuccessful attempt was made to determine cubic Magnus and pitch damping moment coefficients from the range data. Figures 27 and 28 are plots of the raw range values as obtained from the epicyclic reduction.

Figure 27 shows that the Magnus moment is positive for Mach numbers exceeding 1.6, and negative for lower speeds. The positive Magnus moment at high supersonic speeds produces a mild undamping of the fast epicyclic arm, but the effect of decreasing Mach number during flight is to convert the undamped fast arm to a damped, or stable motion.

Figure 28 shows a negative value for  $C_{M_q} + C_{M_\alpha}$ , at all Mach numbers above 0.8. Since a negative value of the pitch damping moment coefficient is stabilizing, Figure 28 predicts good damping at transonic and supersonic Mach numbers. The small positive value of  $C_{M_q} + C_{M_\alpha}$ , at Mach number 0.8, produces a mild undamping of the slow epicyclic arm at that speed.

The sparsity of Magnus and pitch damping data in the present tests, and the observed data scatter in Figures 27 and 28 suggest that these results are more qualitative than quantitative, and should be used accordingly.

#### D. Damping Rates

Figures 29 and 30 show the observed XM712 epicyclic damping rates, for the fast and slow arms, respectively. The fast arm, which turns in the same direction as missile roll, shows a mild instability at Mach numbers above 1.7, at the small yaw levels tested. The slow arm (Figure 30), which rotates in the opposite direction to missile roll, is damped at all supersonic speeds, and shows a mild instability at subsonic speeds.

For a projectile launched at a Mach number of 1.8, the fast arm instability indicated in Figure 29 will soon disappear, due to decreasing Mach number along the flight path. Thus the XM712, launched at any supersonic zone should exhibit dynamically stable flight over the supersonic region. As the projectile approaches transonic speed, Figure 30 predicts a mild, but slowly growing dynamic instability in the slow arm, thus confirming the possible existence of a slow arm limit-cycle yaw at subsonic speeds. Unfortunately, the yaw levels achieved in the present tests are too small to permit any estimate of the size of the limit-cycle, if it exists at all; thus, the BRL test results neither confirm or deny the WSMR telemetry data showing "coning motion."

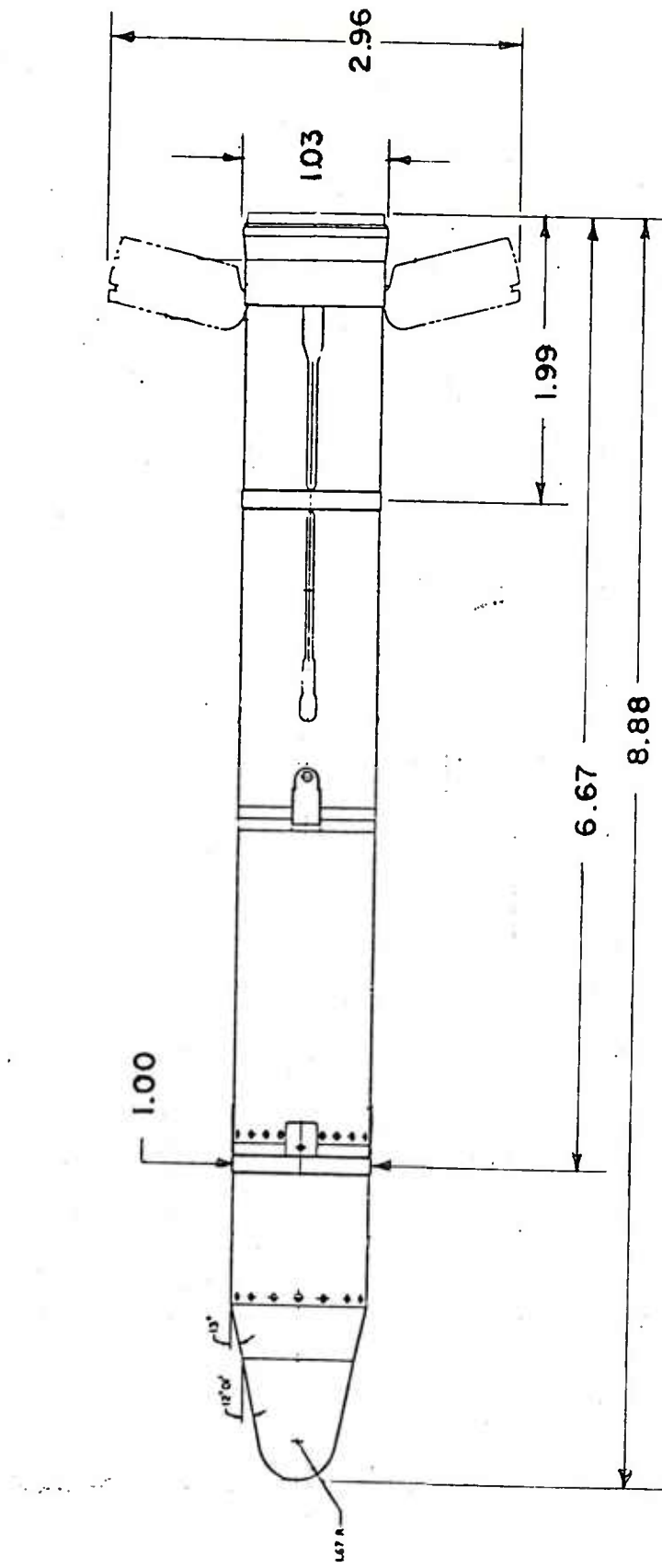
#### IV. CONCLUSIONS

The B040 projectiles have the highest drag coefficient of the three model types tested. The B035 models showed the least drag, and the B035 MOD drag coefficient was midway between that of the other two model types. The drag difference between model types is roughly 2%, at all Mach numbers tested. The B040 model shows 8% less drag than the wind tunnel values at subsonic speeds; at low supersonic speeds, the range data are approximately 3% above the wind tunnel curve, and for Mach numbers above 1.5, the range and wind tunnel data are in close agreement.

The range data show that both the B035 and the B035 MOD configurations approach neutral stability at a Mach number of 1.5, for small angles of attack. The B040 configuration is more stable at all supersonic speeds, and probably will approach neutral stability at a Mach number around 1.8. The range pitching moment coefficients agree with wind tunnel values at subsonic and transonic speeds.

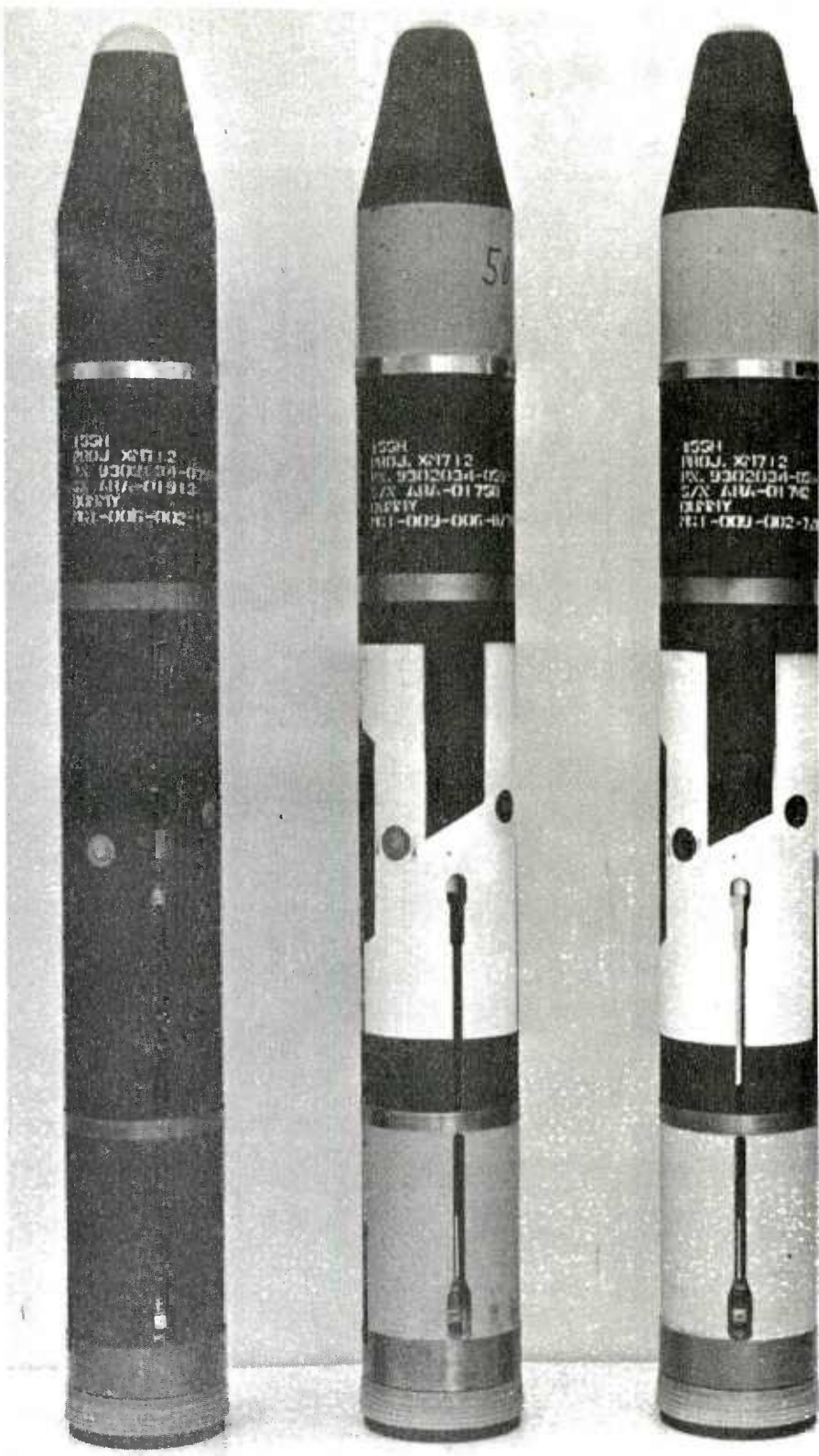
The range values of normal force coefficient are sparse, and less well determined than the pitching moment data. The available normal force coefficient data from the range show roughly 20% less normal force than the wind tunnel curve, at supersonic speeds. The only available subsonic normal force data point from the range agrees with the wind tunnel value.

A mild fast arm dynamic instability was observed above Mach number 1.7. However, decreasing Mach number along the trajectory results in an early disappearance of the instability, and the XM712 projectile should therefore exhibit generally dynamically stable flight at all supersonic zones. The slow arm shows a mild but increasing dynamic instability at transonic and subsonic speeds at small angles of attack, which confirms the possible existence of limit-cycle or "coning" motion. Unfortunately, the small yaw levels attained in the present tests do not permit an estimate of the size of a limit-cycle, if it exists at all. Thus the BRL tests neither confirm nor deny the WSMR telemetry data showing "coning motion."



ALL DIMENSIONS IN CALIBERS  
(1 CALIBER = 154.7mm)

Figure 1. Sketch of the XM712 Projectile



BO 40

BO 35 MOD

BO 35

Figure 2. Photograph of XM712 Projectiles

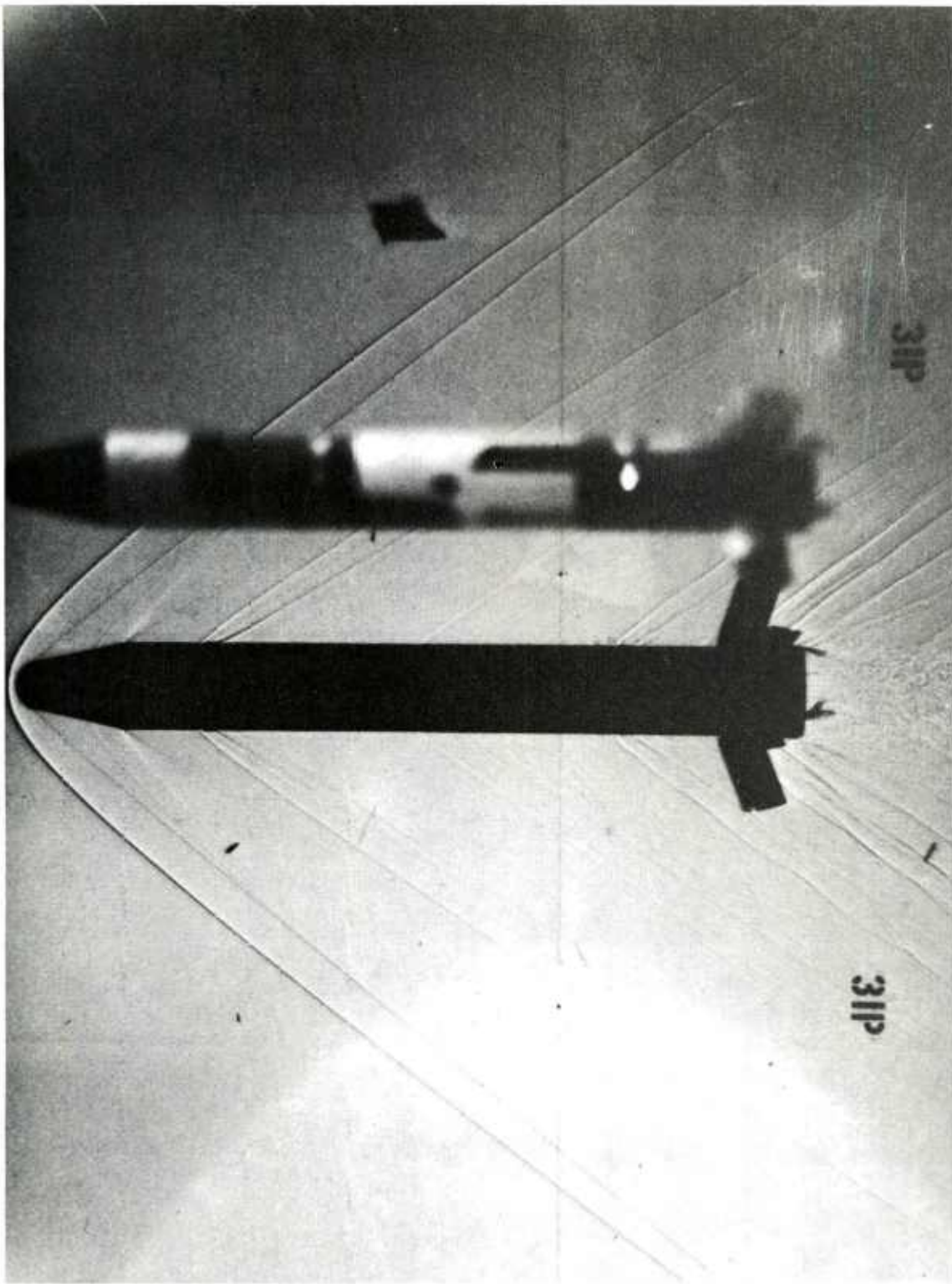


Figure 5. Shadowgraph of BO 35 Model at Mach 1.78

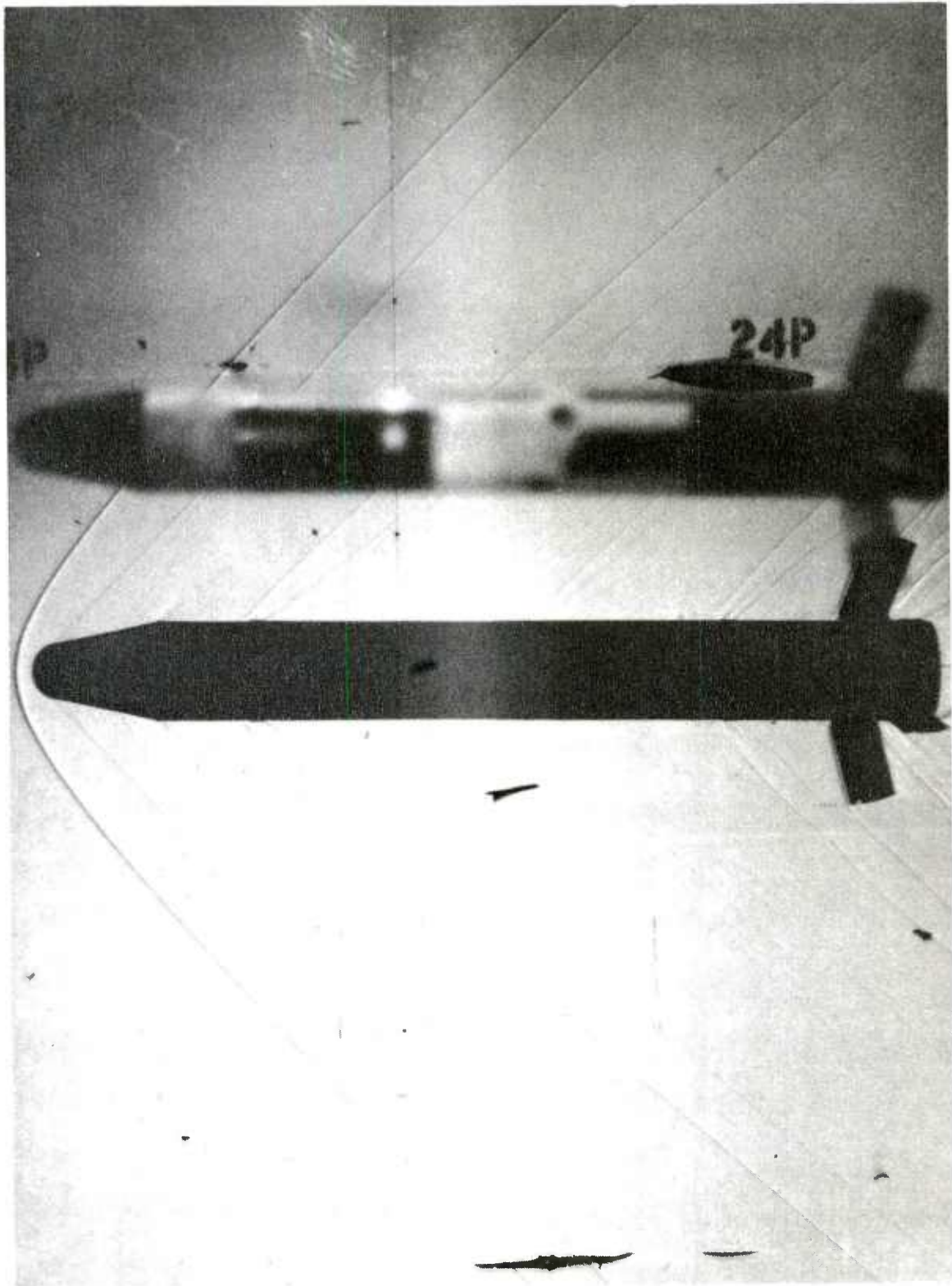


Figure 4. Shadowgraph of BO 35 MOD Model at Mach 1.48

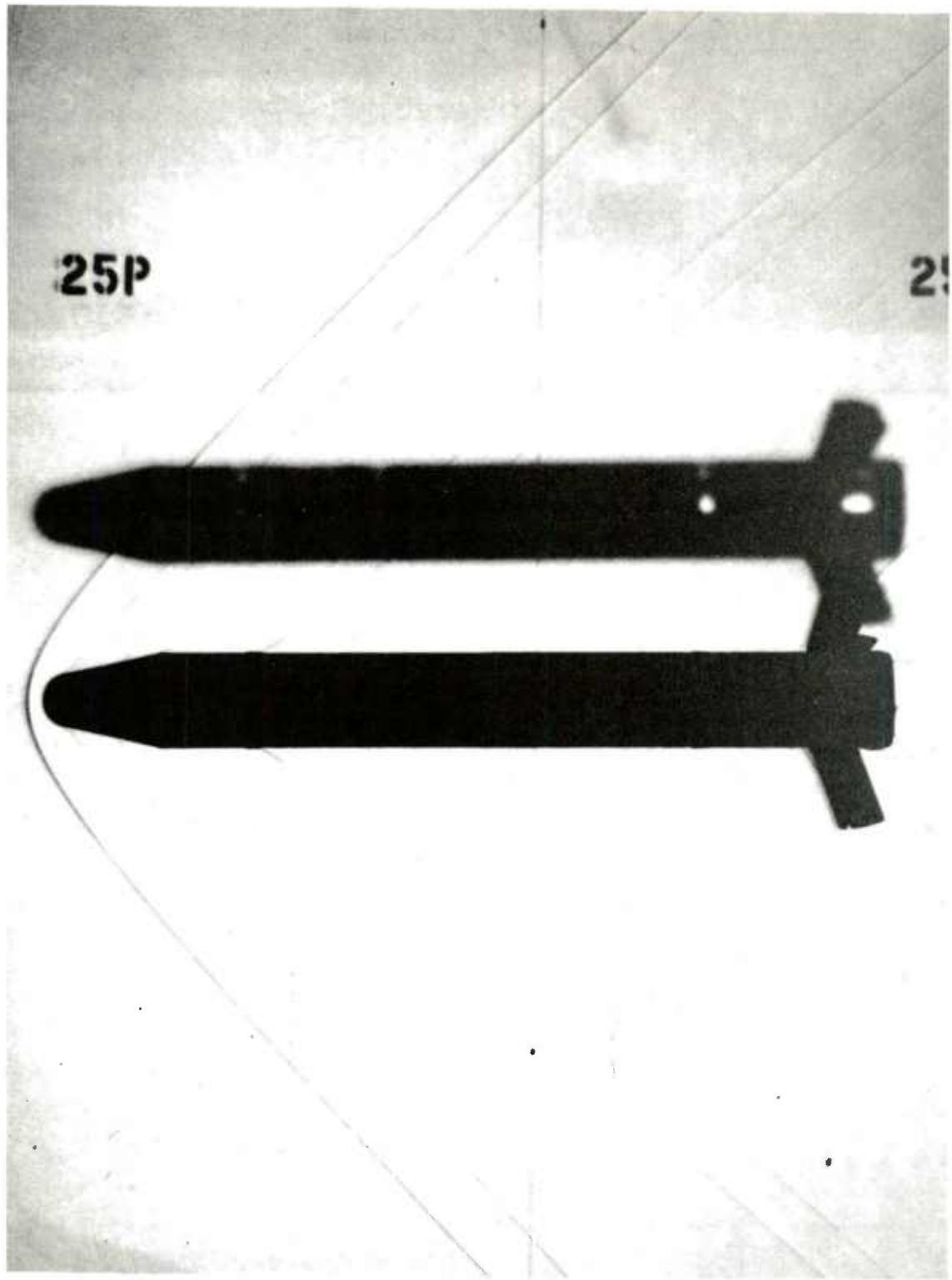


Figure 5. Shadowgraph of BO 40 Model at Mach 1.49

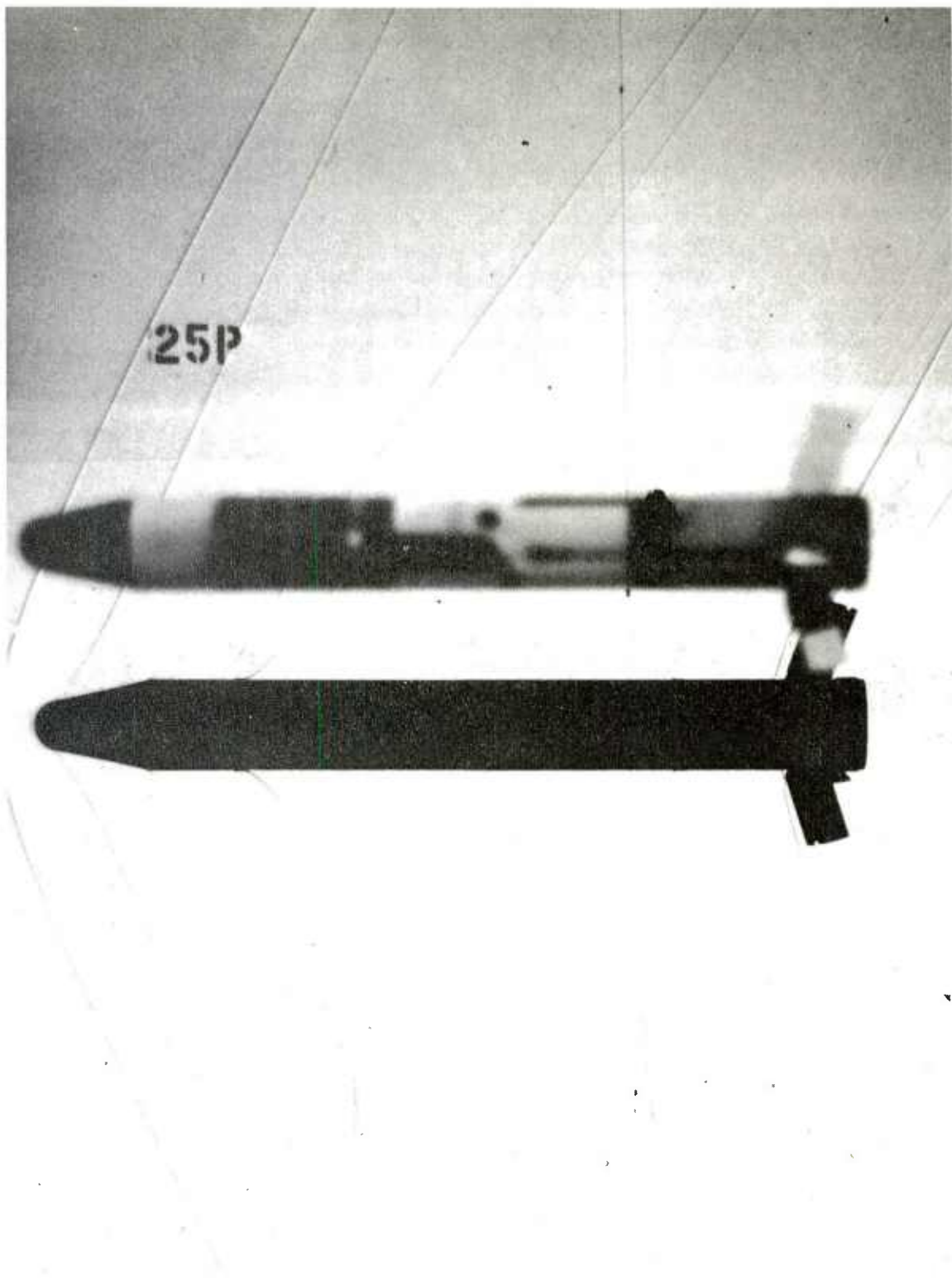


Figure 6. Shadowgraph of BO 35 Model at Mach 1.20

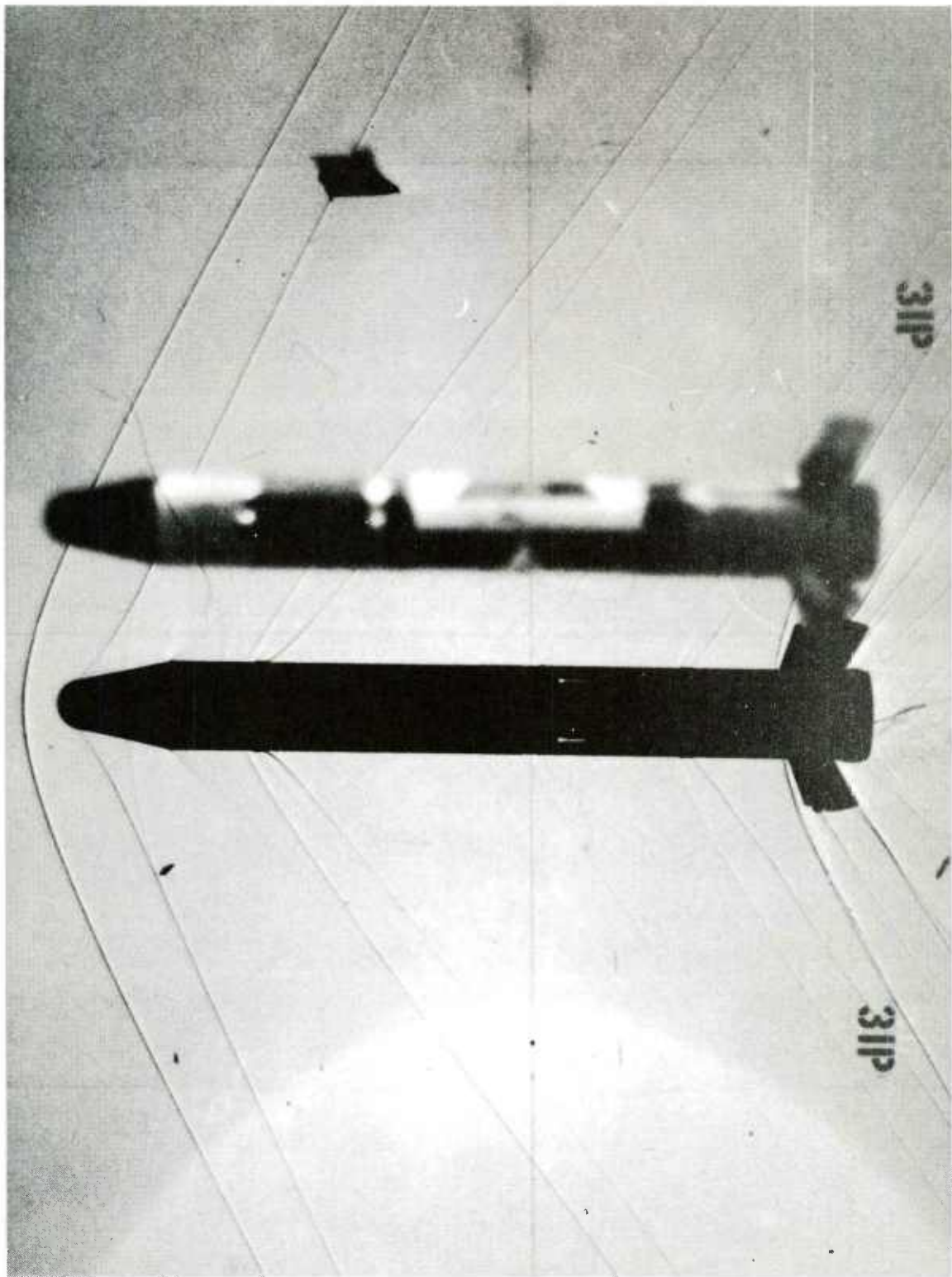


Figure 7. Shadowgraph of BO 35 MOD Model at Mach 1.19

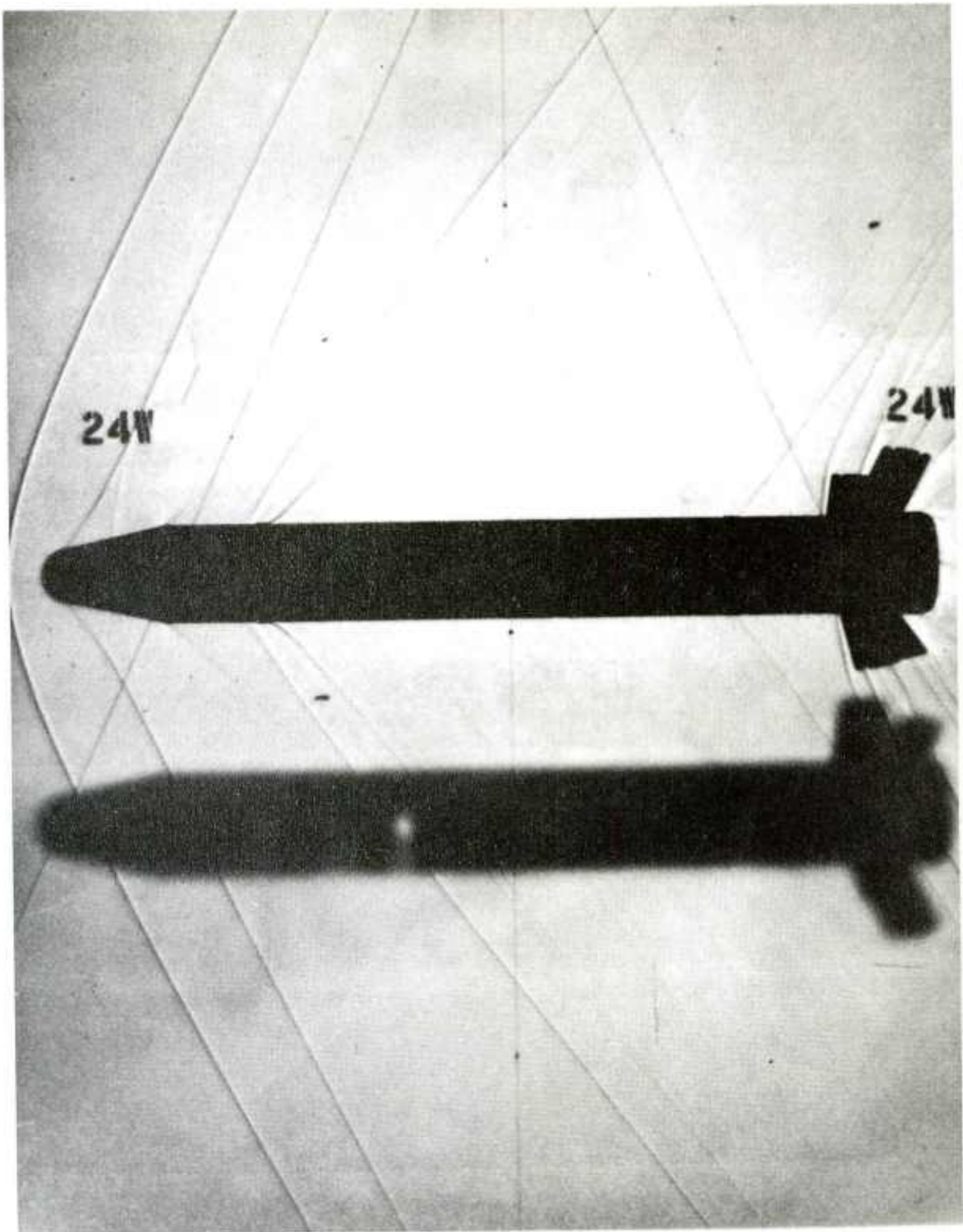


Figure 8. Shadowgraph of BO 40 Model at Mach 1.20

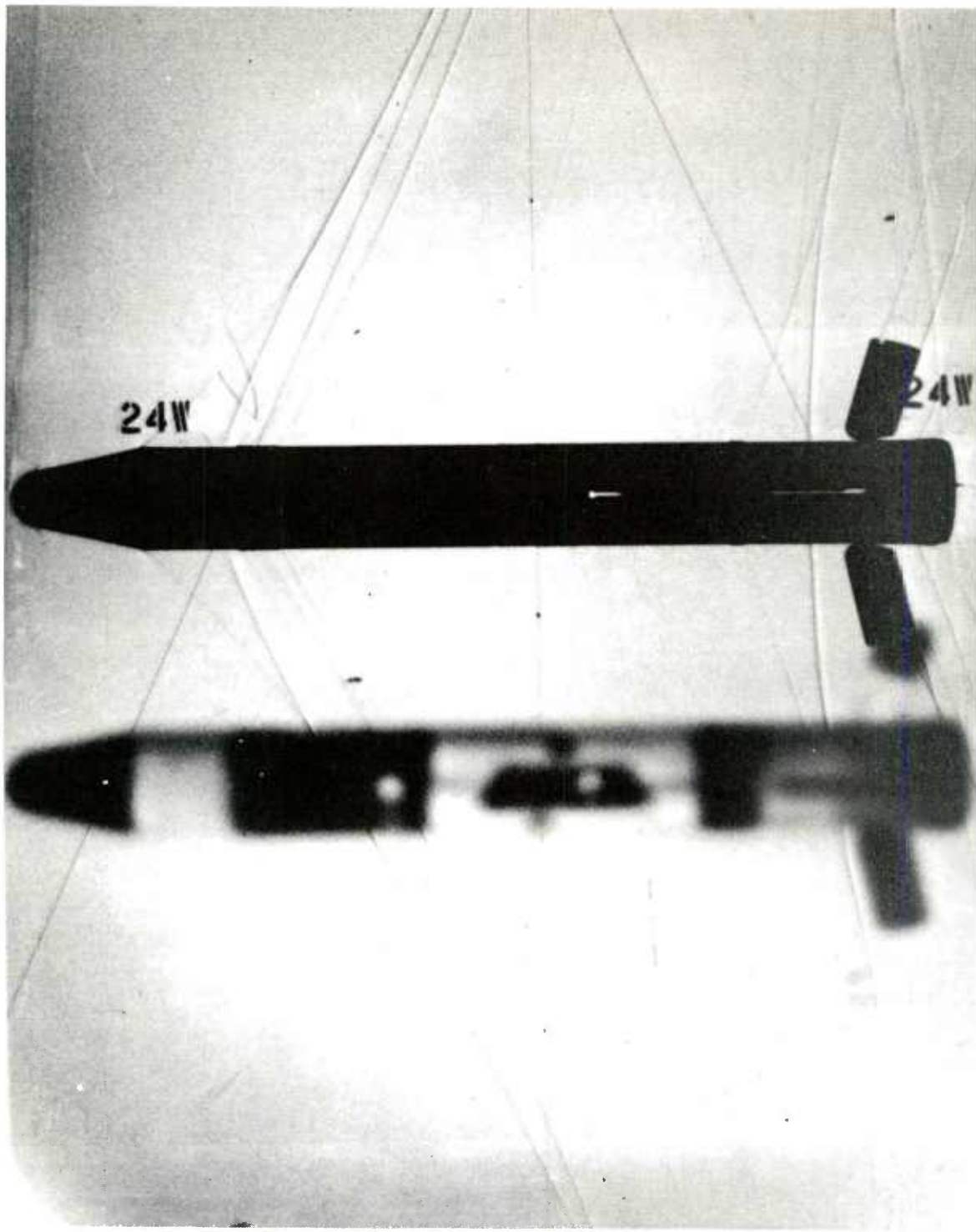


Figure 9. Shadowgraph of B0 35 Model at Mach 1.04

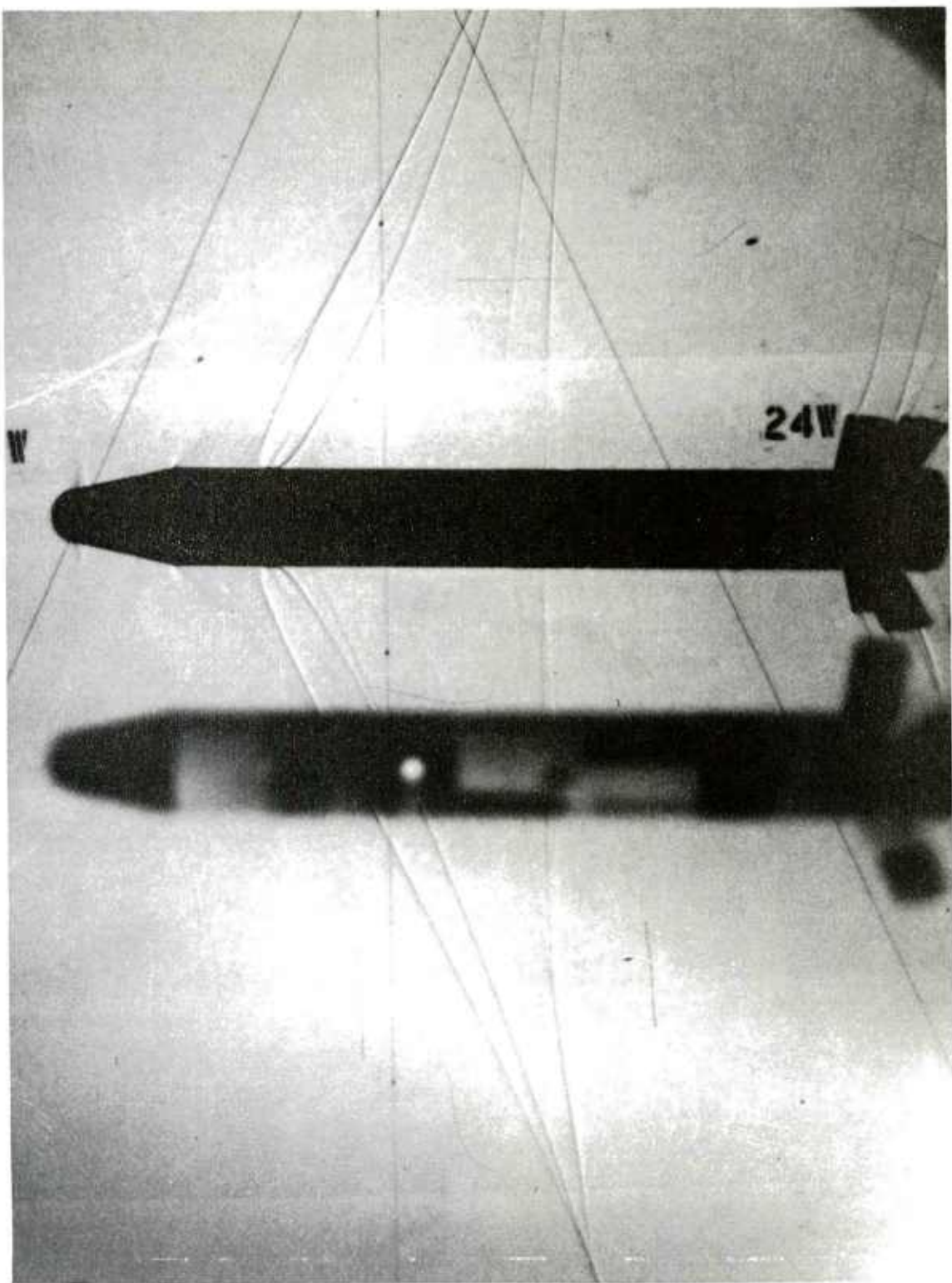


Figure 10. Shadowgraph of BO 35 MOD Model at Mach 1.02

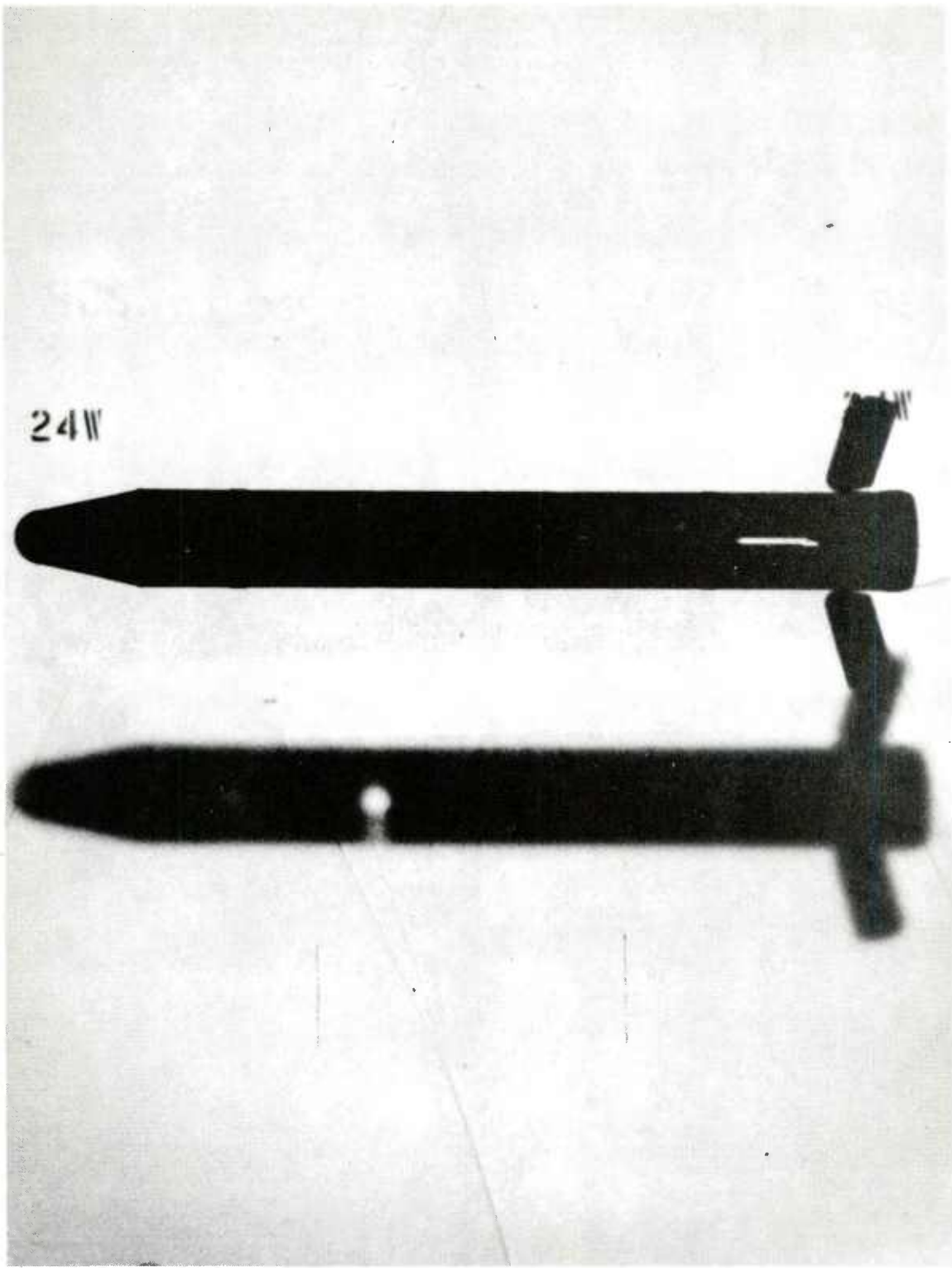


Figure 11. Shadowgraph of BO 40 Model at Mach 1.01

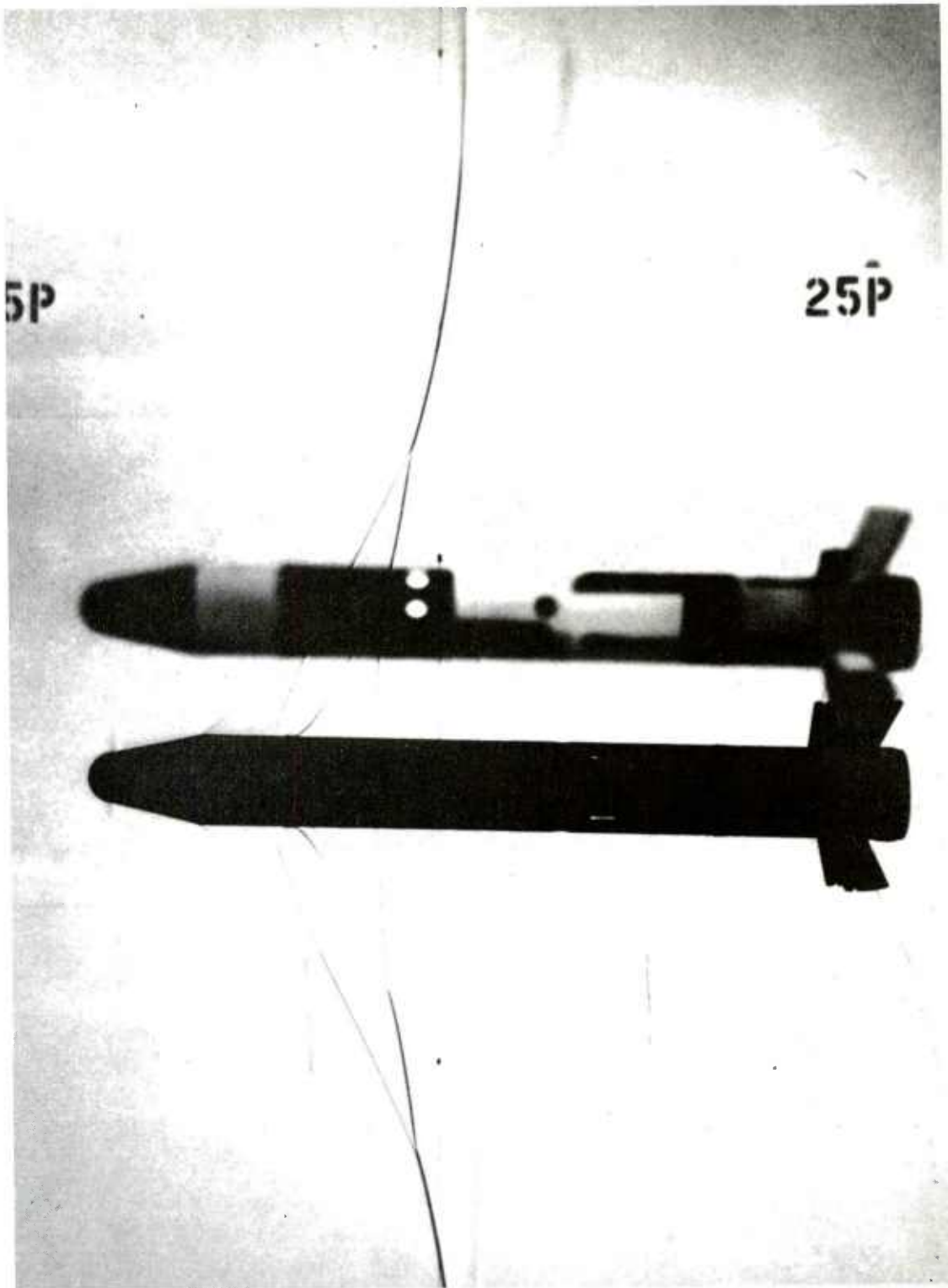


Figure 12. Shadowgraph of BO 35 Model at Mach 0.98

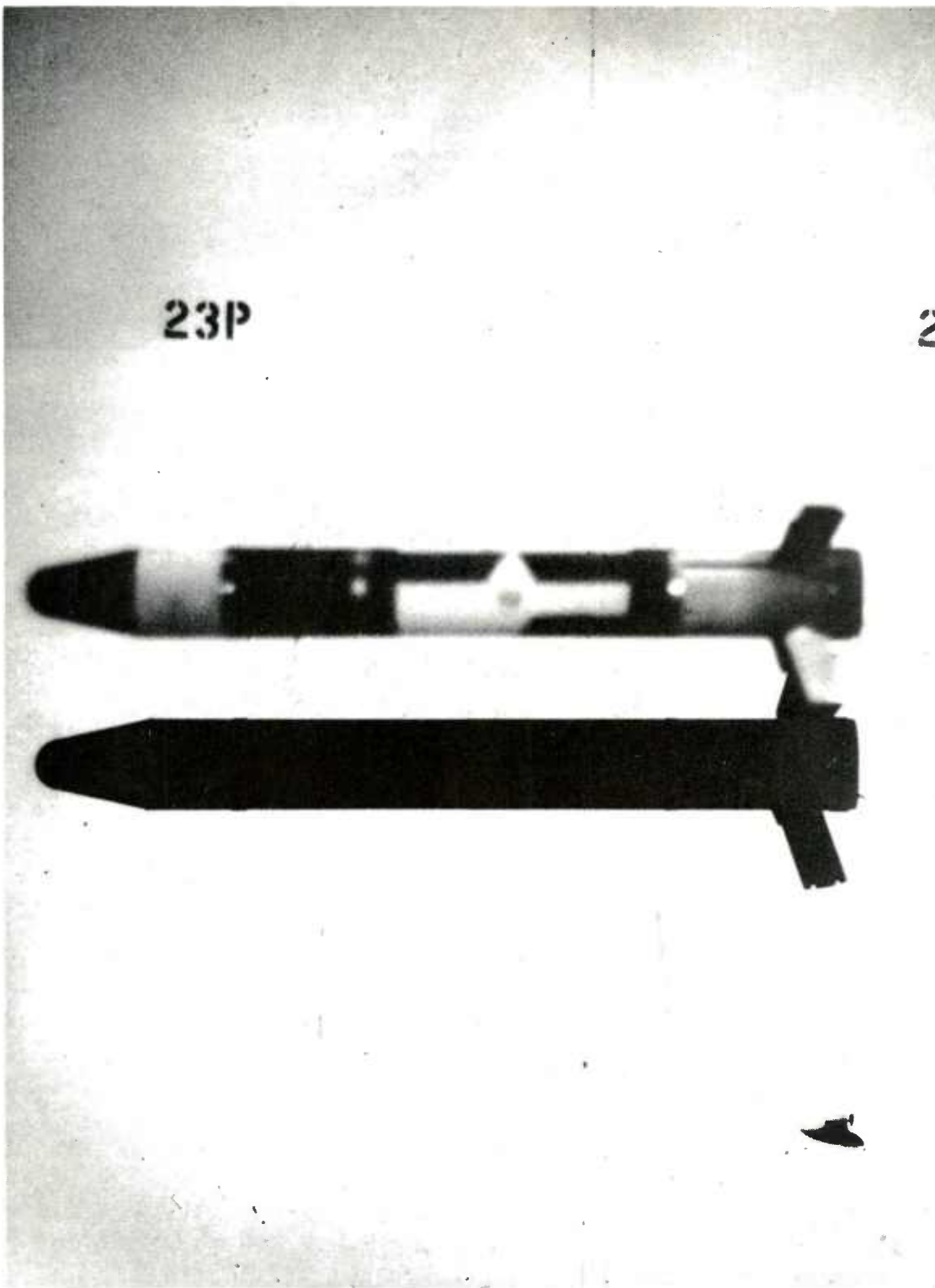


Figure 13. Shadowgraph of BO 35 MOD Model at Mach 0.97

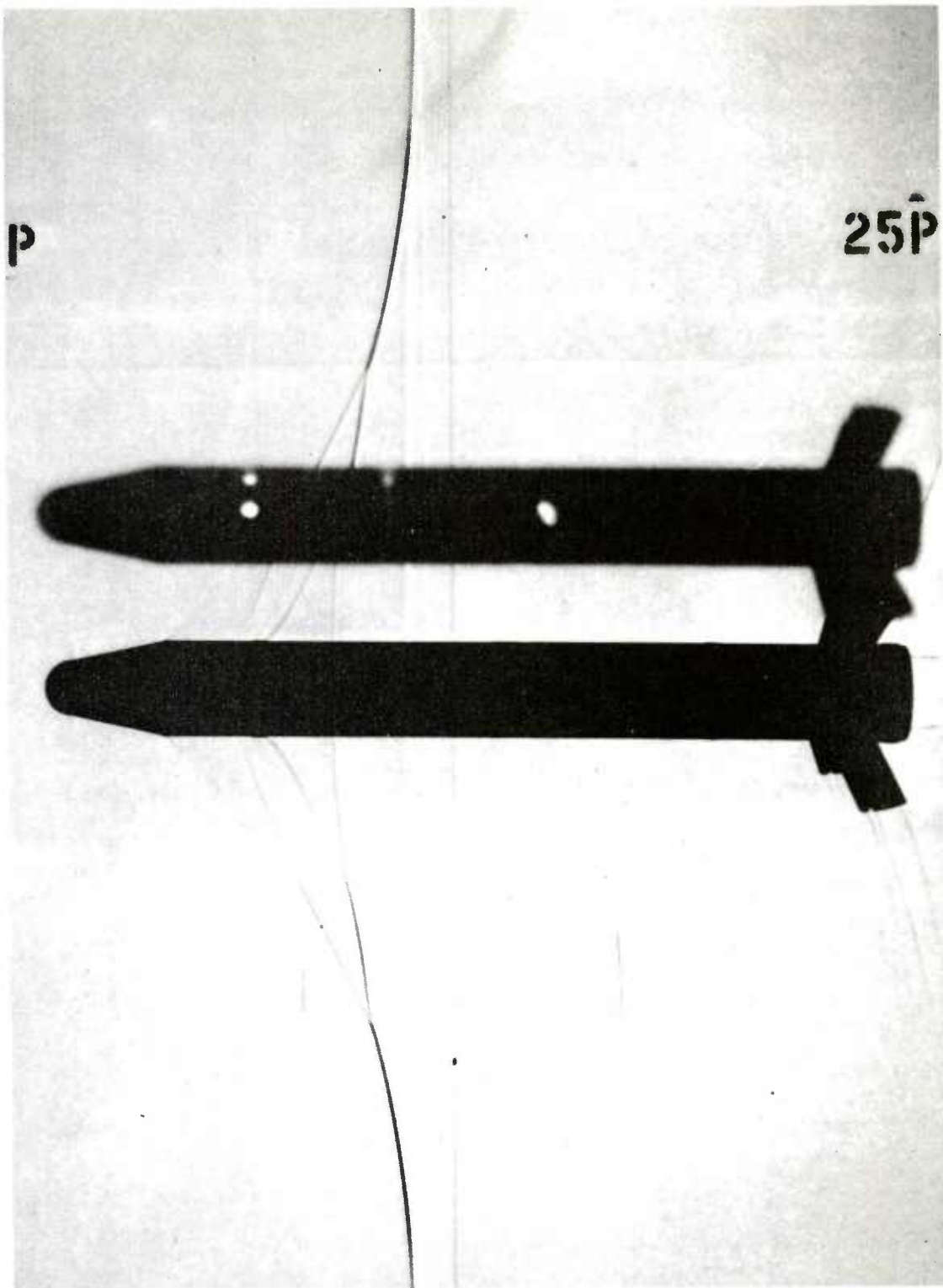


Figure 14. Shadowgraph of BO 40 Model at Mach 0.98

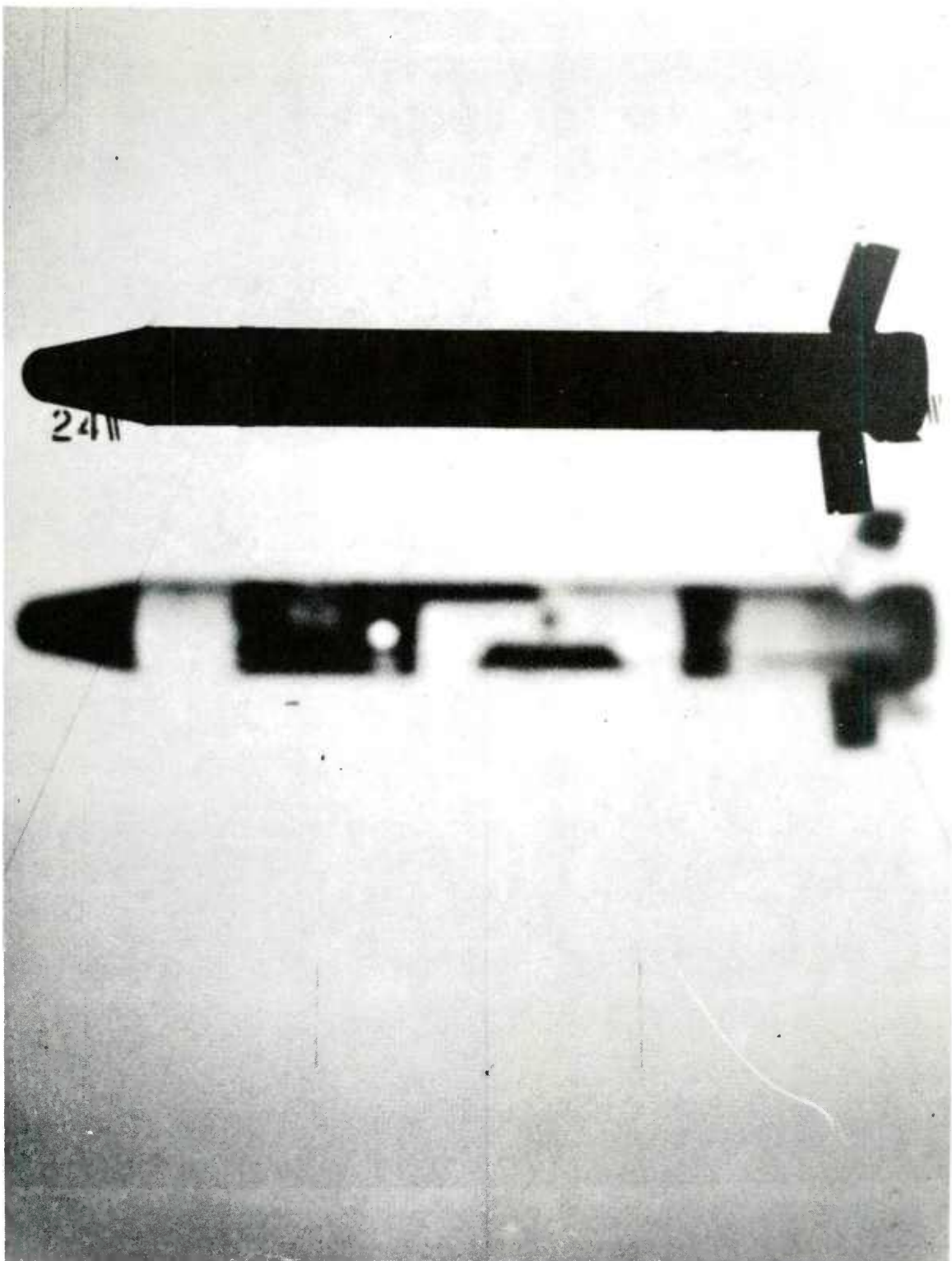


Figure 15. Shadowgraph of BO 35 Model at Mach 0.81

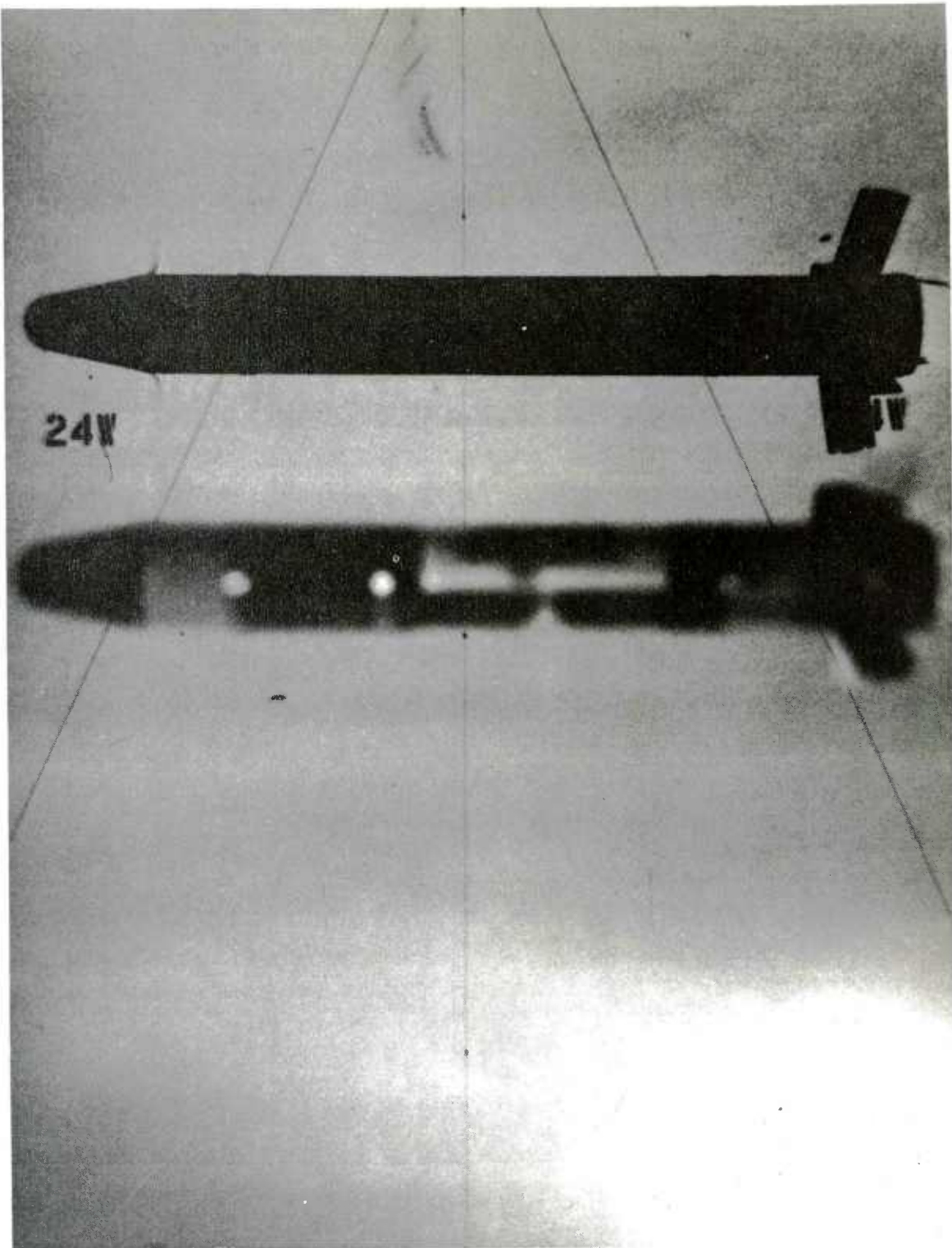


Figure 16. Shadowgraph of BO 35 MOD Model at Mach 0.80

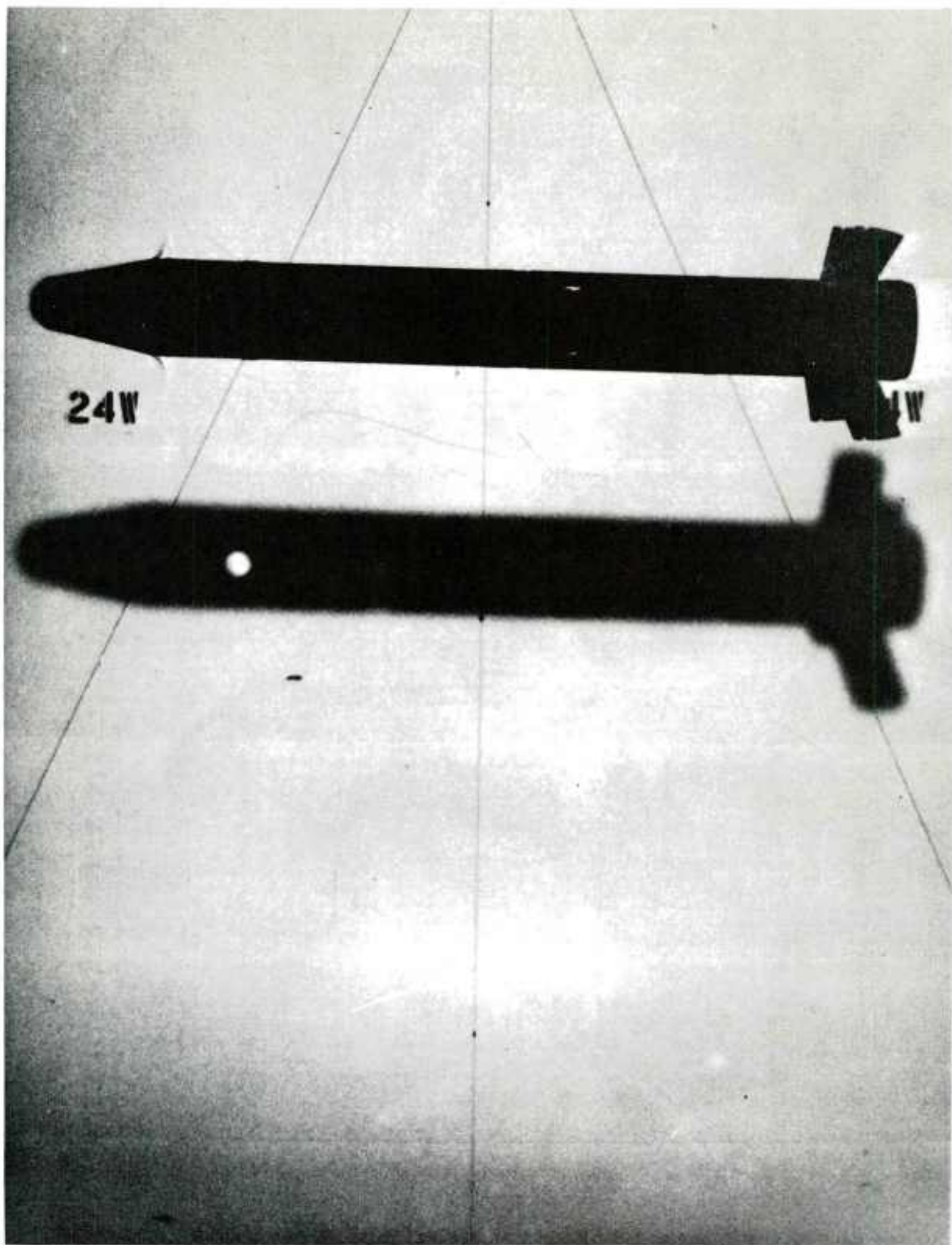


Figure 17. Shadowgraph of BO 40 Model at Mach 0.81

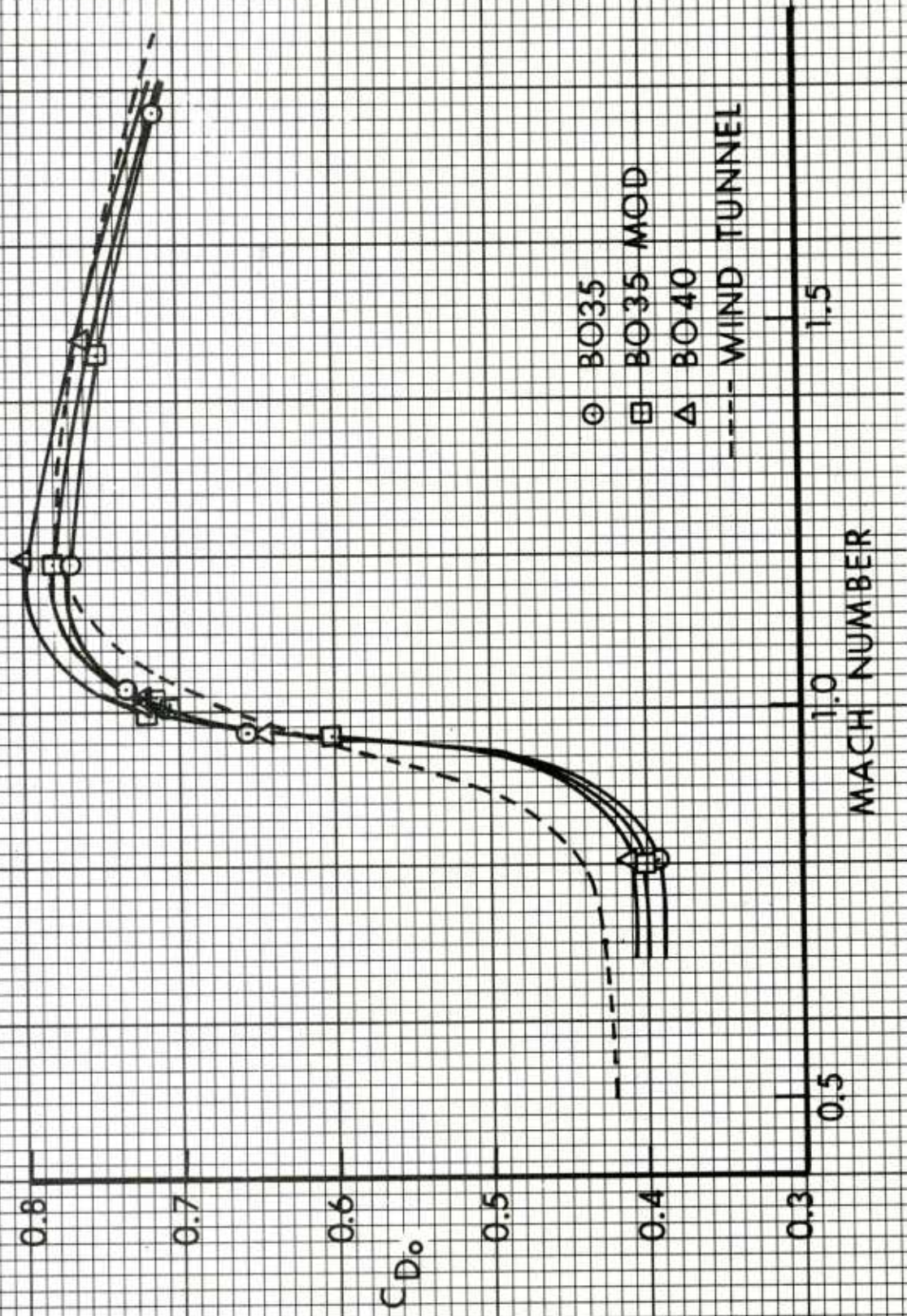


Figure 18. Zero-Yaw Drag Force Coefficient versus Mach Number



Figure 19. Quadratic Yaw Drag Force Coefficient versus Mach Number

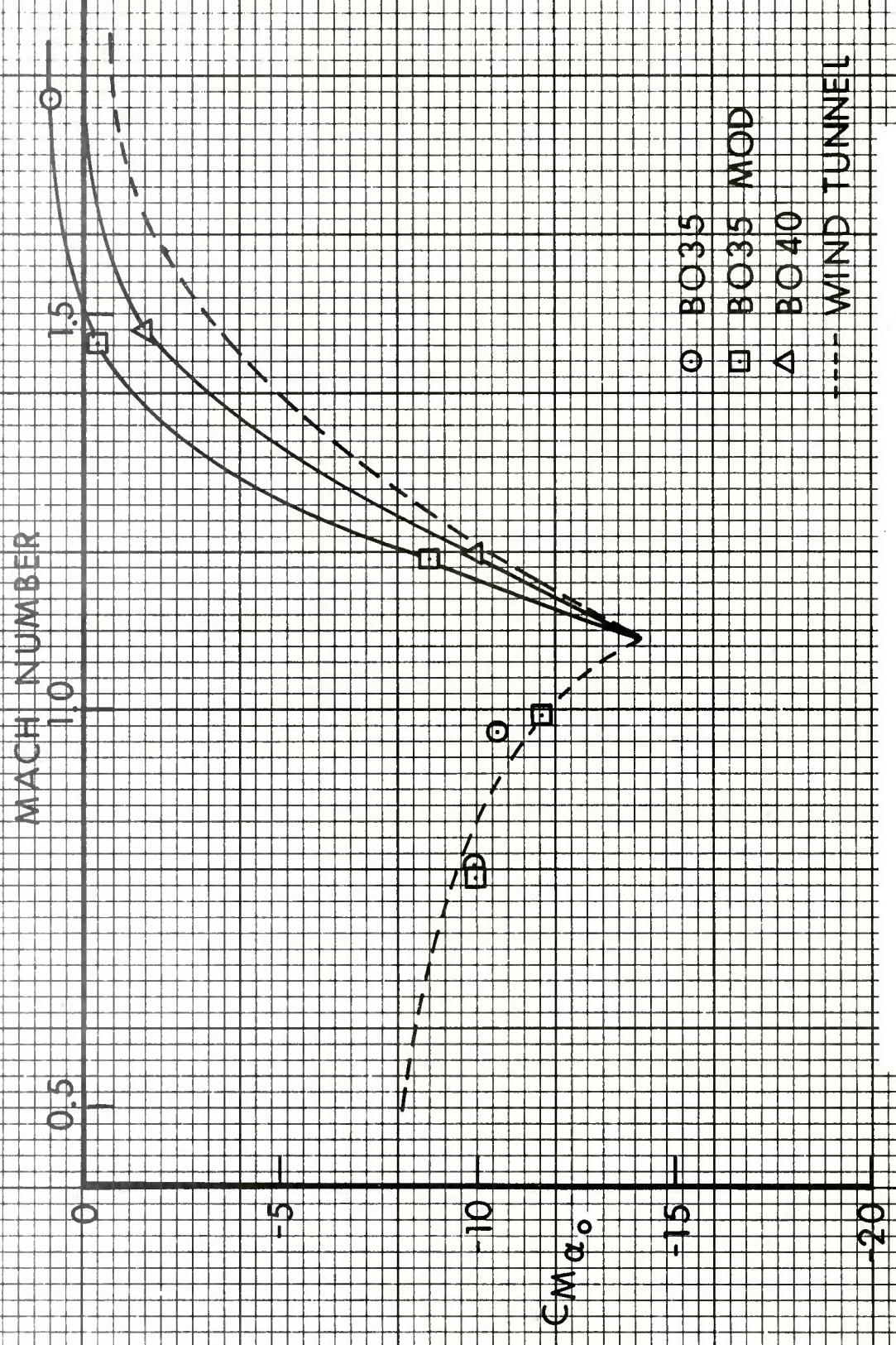


Figure 20. Zero-Yaw Pitching Moment Coefficient versus Mach Number

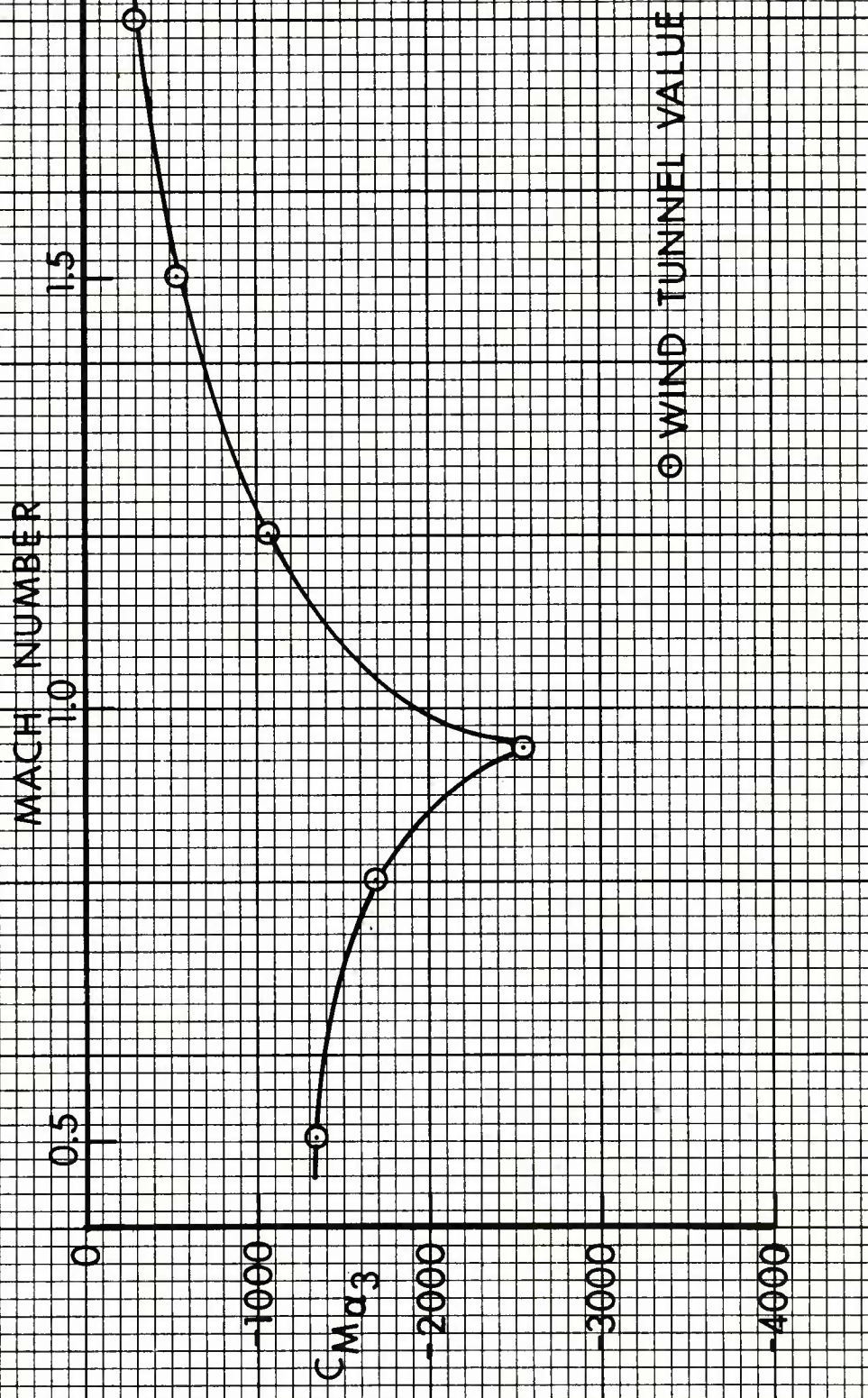


Figure 21. Cubic Pitching Moment Coefficient versus Mach Number

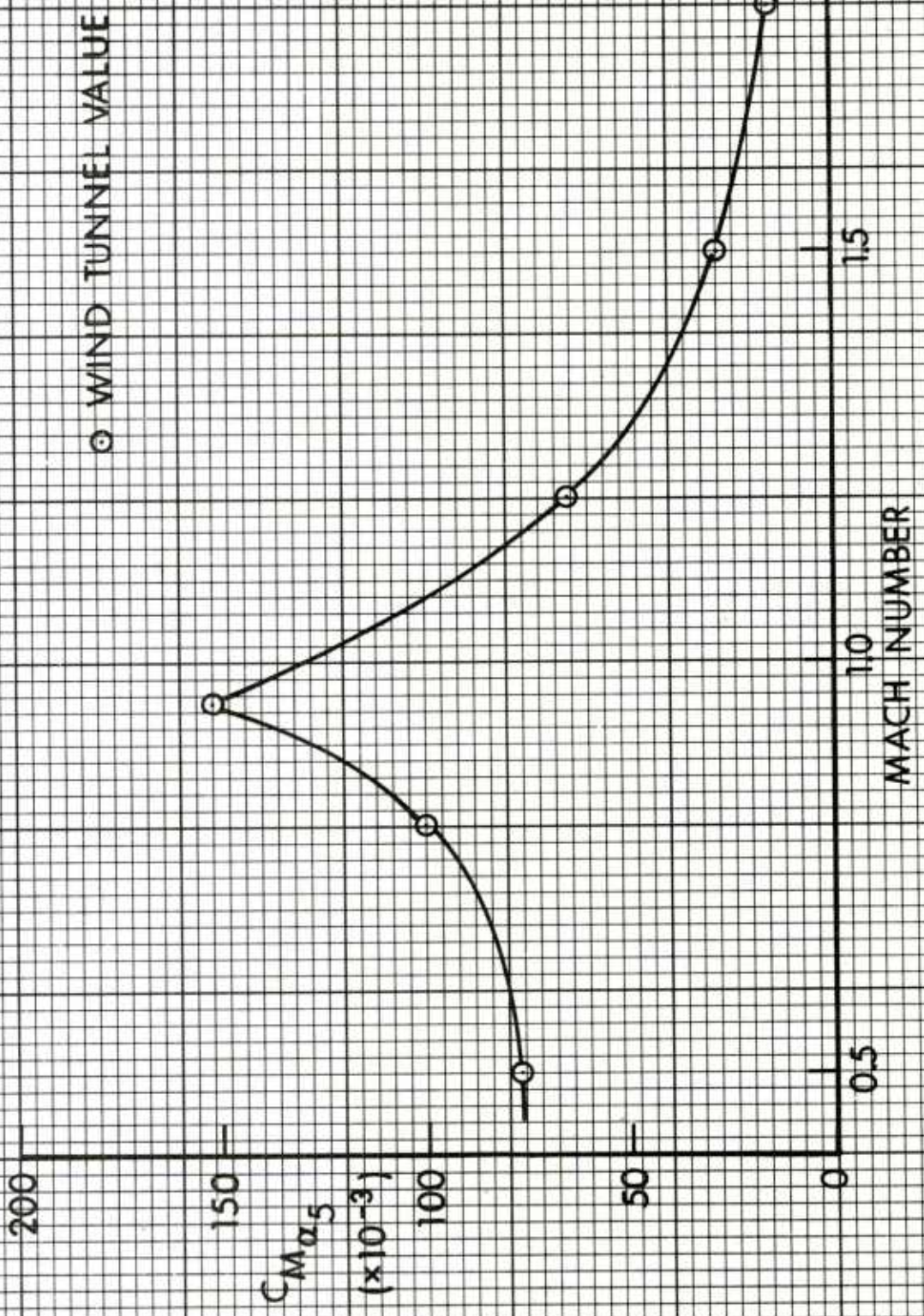


Figure 22. Quintic Pitching Moment Coefficient versus Mach Number

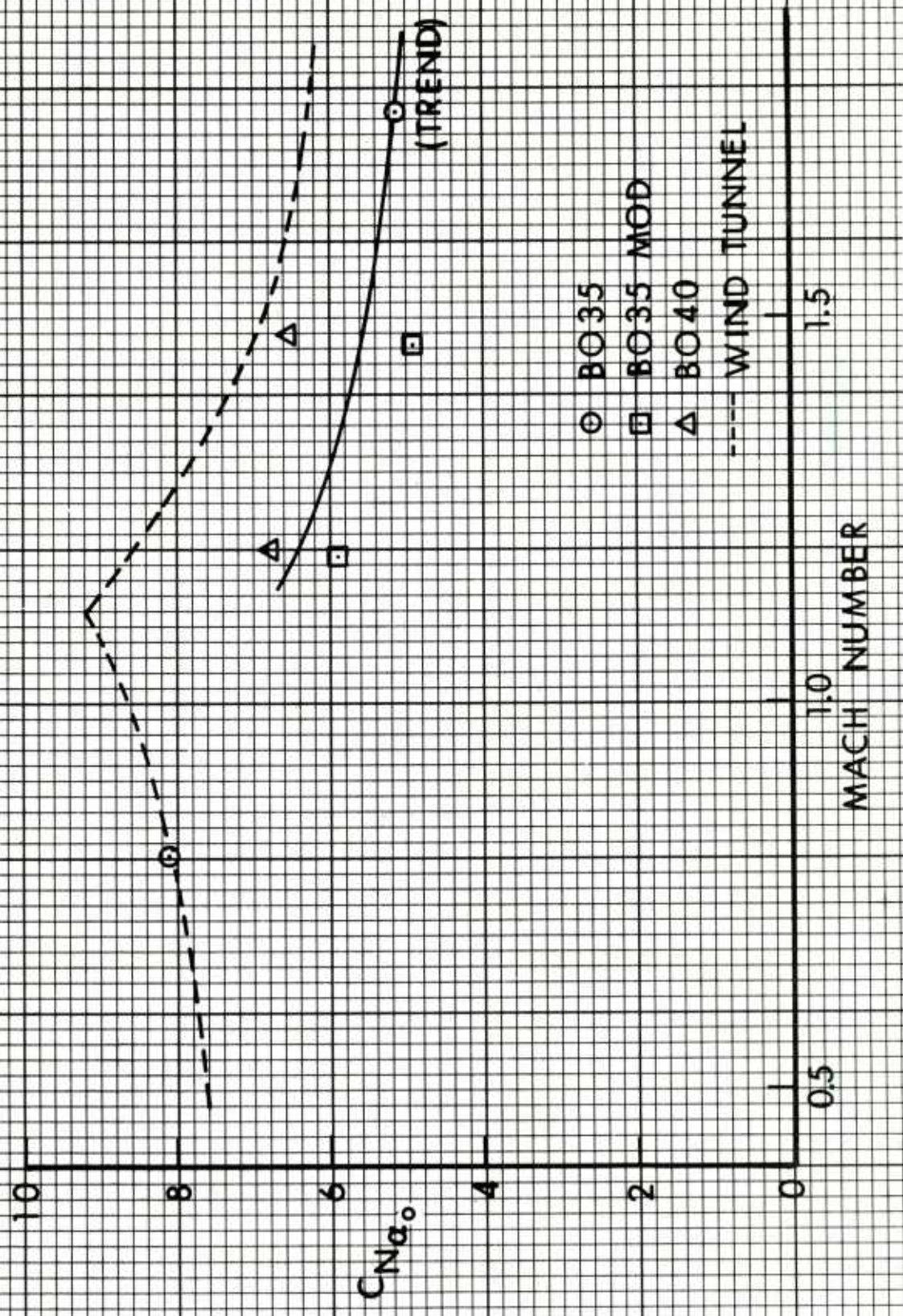


Figure 23. Zero-Yaw Normal Force Coefficient versus Mach Number

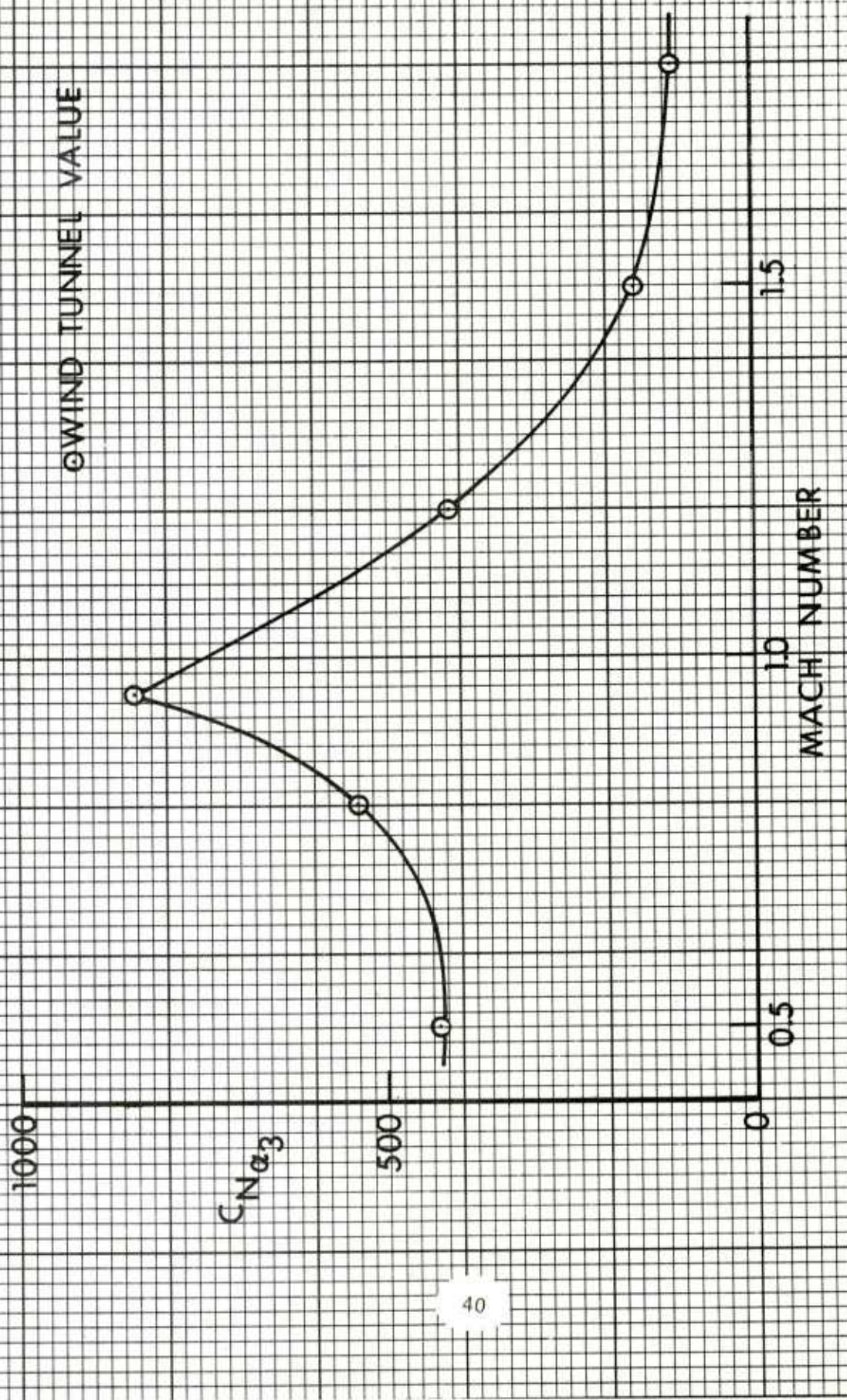


Figure 24. Cubic Normal Force Coefficient versus Mach Number

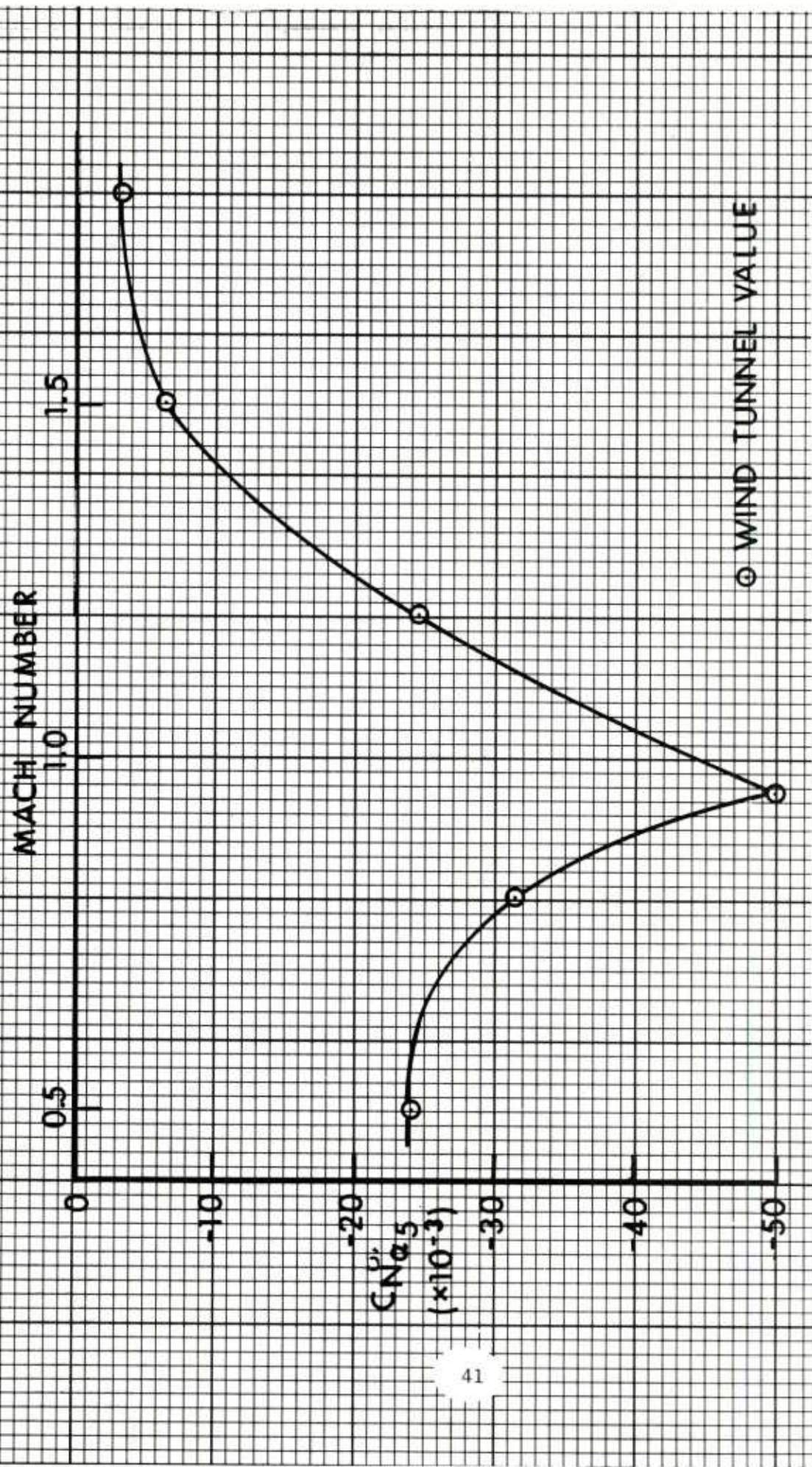


Figure 25. Quintic Normal Force Coefficient versus Mach Number

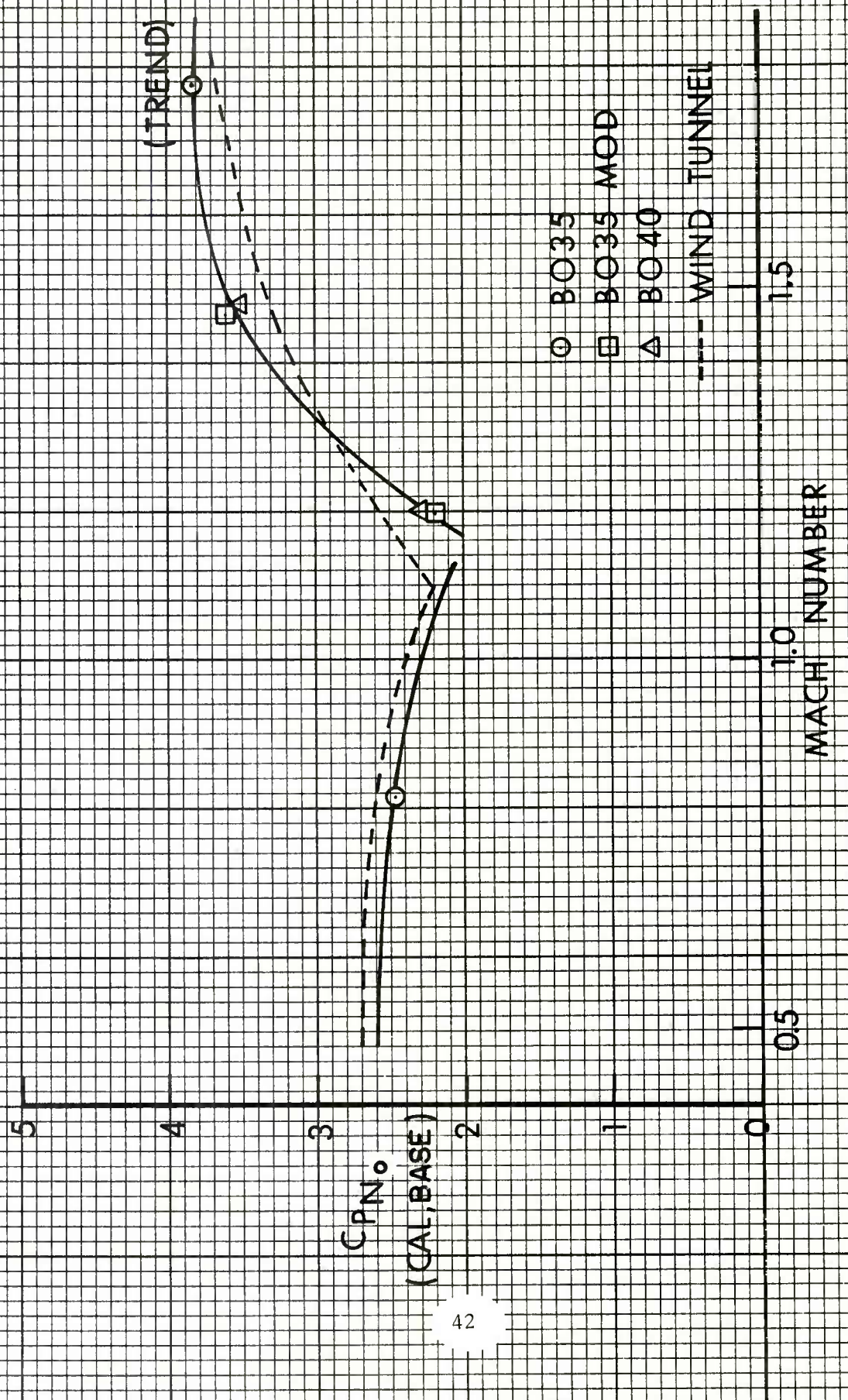


Figure 26. Zero-Yaw Center of Pressure versus Mach Number

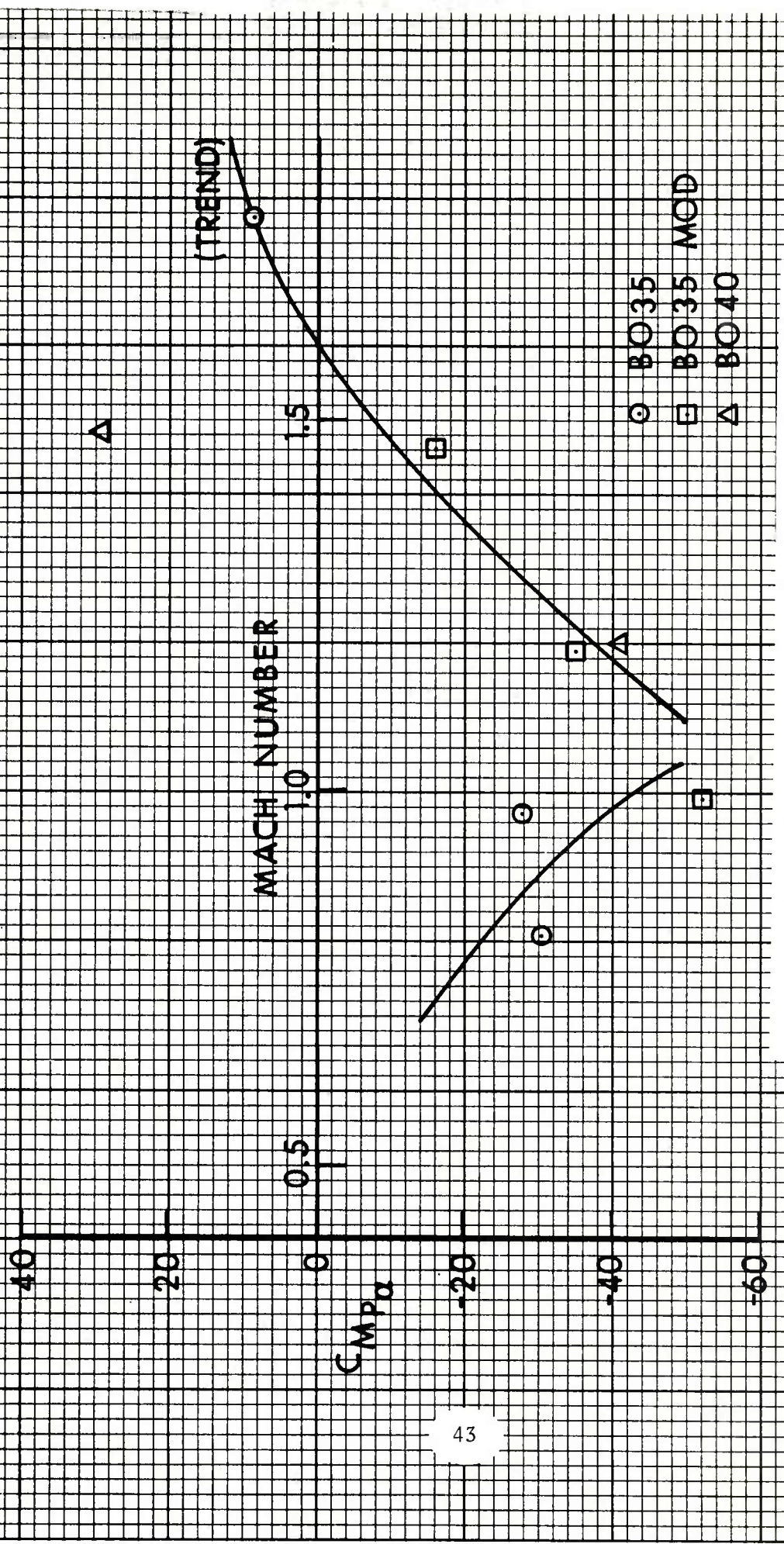


Figure 27. Magnus Moment Coefficient versus Mach Number

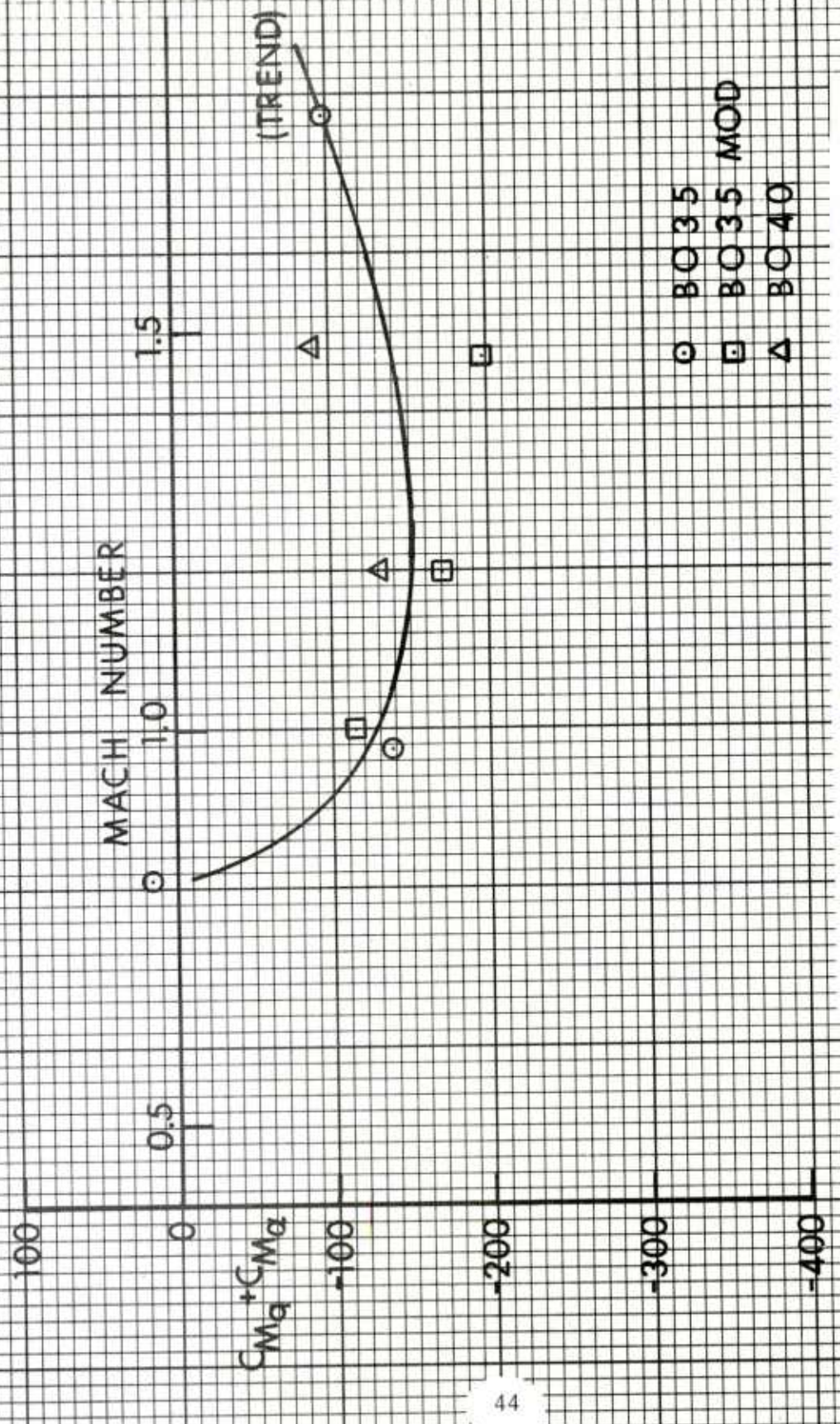


Figure 28. Pitch Damping Moment Coefficient versus Mach Number

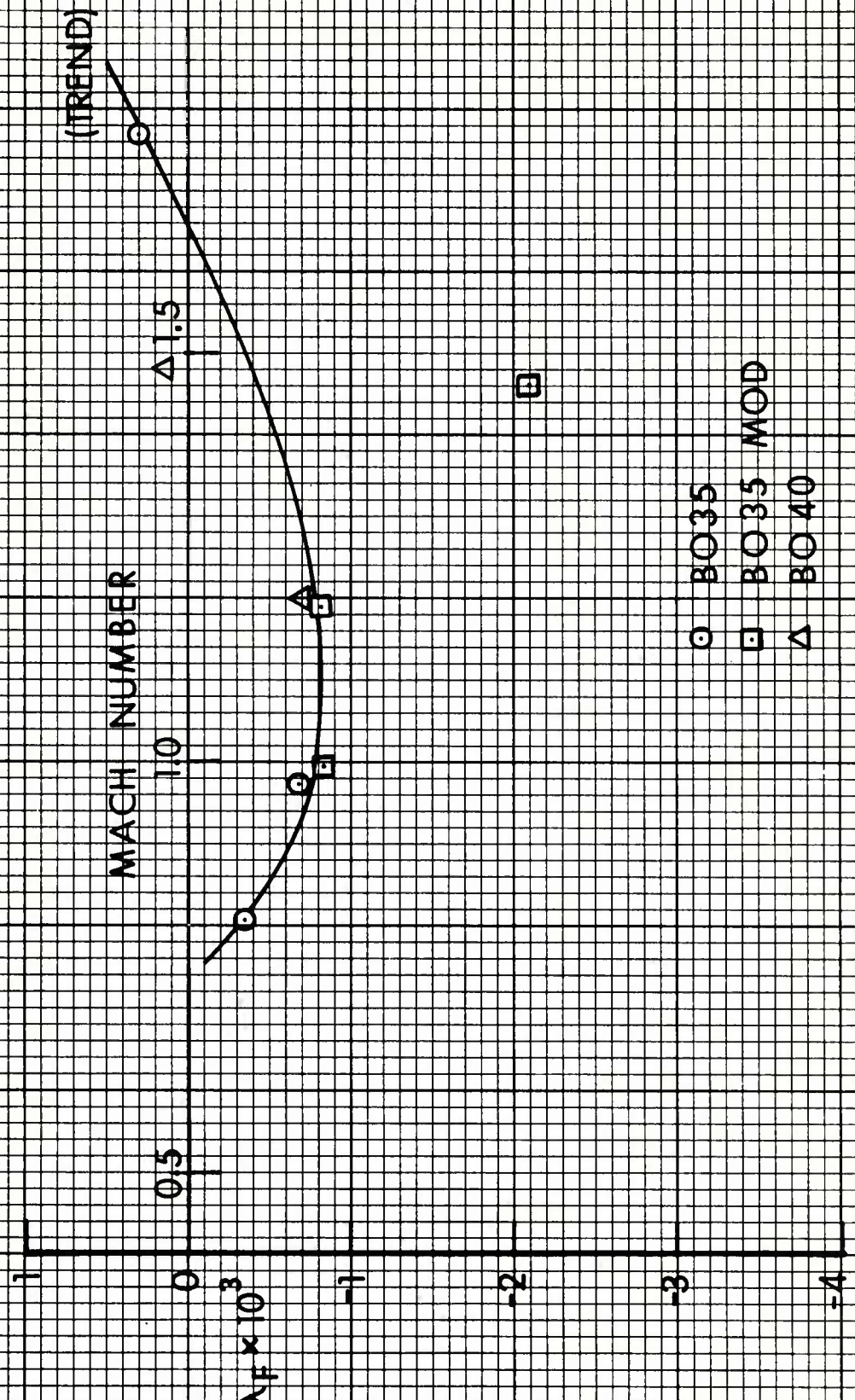


Figure 29. Fast Arm Damping Rate versus Mach Number

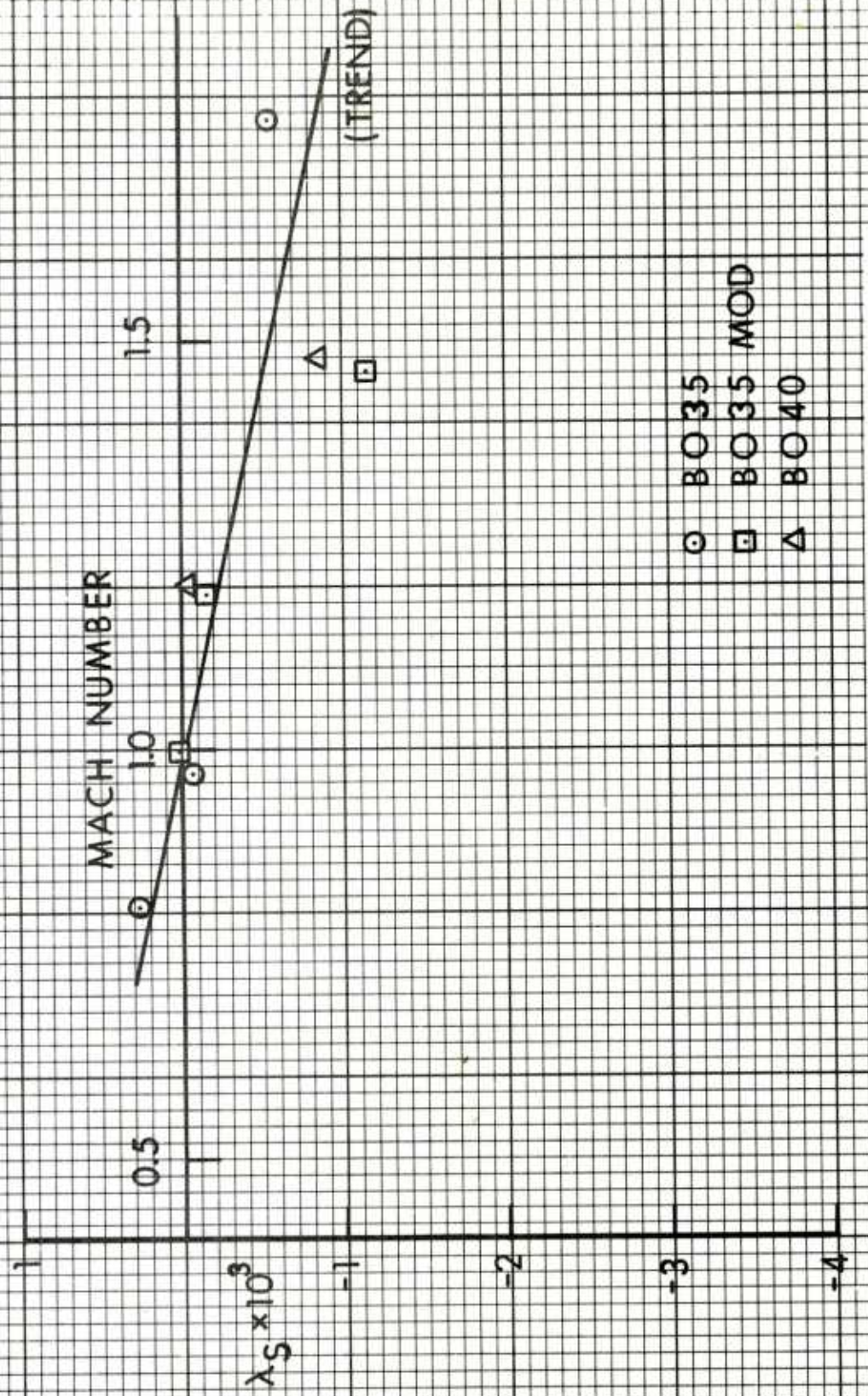


Figure 30. Slow Arm Damping Rate versus Mach Number

TABLE I. PHYSICAL CHARACTERISTICS

Model Type	m (kg)	d (m)	l (cal)	$I_x$ (kg.m <sup>2</sup> )	$I_y$ (kg.m <sup>2</sup> )	c.m. (cal.-base)
BO 35	62.69	.1547	8.88	.2505	8.470	3.71
BO 35 MOD	62.78	.1547	8.88	.2507	8.463	3.71
BO 40	62.63	.1547	8.88	.2491	8.184	3.75

TABLE II. SUMMARY OF AERODYNAMIC CHARACTERISTICS

Round Number	Type	M	$\bar{\alpha}_t$ (deg)	$C_D$	$C_{M\alpha}$	$C_{N\alpha}$	$C_{P_N}$ (cal.-base)
16519	B035	1.77	2.9	.740	-0.06	5.51	3.69
16484	B035	1.19	0.6	.771	-----	-----	-----
16502	B035	1.03	0.5	.735	-----	-----	-----
16505	B035	0.97	0.9	.660	-11.21	-----	-----
16516	B035	0.81	0.9	.398	-10.56	8.31	2.43
16482	B035 MOD	1.46	1.8	.760	- 0.88	5.07	3.53
16500	B035 MOD	1.19	1.0	.783	- 9.26	6.04	2.17
16974	B035 MOD	1.02	0.6	.715	-----	-----	-----
16973	B035 MOD	1.01	0.4	.709	-----	-----	-----
16503	B035 MOD	1.00	0.7	.723	-12.04	-----	-----
16506	B035 MOD	0.97	0.4	.604	-----	-----	-----
16518	B035 MOD	0.80	0.9	.404	-10.44	-----	-----
16483	B040	1.48	1.2	.763	- 1.87	6.62	3.46
16501	B040	1.20	1.1	.803	-10.52	6.96	2.24
16975	B040	1.02	0.6	.721	-----	-----	-----
16504	B040	1.01	0.4	.724	-----	-----	-----
16507	B040	0.97	0.4	.648	-----	-----	-----
16517	B040	0.81	0.7	.413	-----	-----	-----

TABLE II. SUMMARY OF AERODYNAMIC CHARACTERISTICS (continued)

Round Number	Type	M	$\bar{\alpha}_T$ (deg)	$C_{M_{P\alpha}}$	$C_{M_q} + C_{M_{\dot{\alpha}}}$
16519	B035	1.77	2.9	9	-99
16484	B035	1.19	0.6	---	-----
16502	B035	1.03	0.5	---	-----
16505	B035	0.97	0.9	-28	-139
16516	B035	0.81	0.9	-31	15
16482	B035 MOD	1.46	1.8	-16	-200
16500	B035 MOD	1.19	1.0	-35	-172
16974	B035 MOD	1.02	0.6	---	-----
16973	B035 MOD	1.01	0.4	---	-----
16503	B035 MOD	1.00	0.7	-52	-116
16506	B035 MOD	0.97	0.4	-----	-----
16518	B035 MOD	0.80	0.9	-----	-----
16483	B040	1.48	1.2	29	- 90
16501	B040	1.20	1.1	-41	-132
16975	B040	1.02	0.6	---	-----
16504	B040	1.01	0.4	---	-----
16507	B040	0.97	0.4	---	-----
16517	B040	0.81	0.7	---	-----

TABLE III. SUMMARY OF FLIGHT MOTION CHARACTERISTICS

Round Number	Type	Muzzle Velocity (m/s)	$\lambda_F \times 10^3$ (1/cal)	$\lambda_S \times 10^3$ (1/cal)	$K_F$	$K_S$	$\phi'_F \times 10^3$ (rad/cal)	$\phi'_S \times 10^3$ (rad/cal)	Roll Rate (deg/m)
16519	B035	619.8	.294	-.568	.039	.031	.94	-.40	6.7
16484	B035	418.2	----	----	.005	.008	----	----	9.4
16502	B035	361.0	----	----	.005	.006	----	----	9.7
16505	B035	338.4	-.699	-.057	.010	.011	7.99	-7.00	12.4
16516	B035	278.9	-.363	.261	.012	.011	7.76	-6.83	11.7
16482	B035 MOD	516.3	-2.113	-1.165	.016	.022	2.67	-1.98	8.7
16500	B035 MOD	416.2	-.831	-.173	.010	.014	7.09	-6.36	9.0
50	16974	B035 MOD	361.7	----	----	.005	.008	----	----
16973	B035 MOD	361.6	----	----	----	.005	.005	----	----
16503	B035 MOD	348.3	-.833	.006	.009	.008	8.03	-7.30	9.2
16506	B035 MOD	336.7	----	----	.006	.003	----	----	10.5
16518	B035 MOD	277.3	----	----	.009	.012	7.66	-6.72	11.7
16483	B040	517.6	.123	-.865	.019	.008	3.46	-2.80	8.1
16501	B040	418.6	-.697	-.053	.012	.015	7.63	-6.97	8.0
16975	B040	363.4	----	----	.001	.010	----	----	----
16504	B040	350.5	----	----	.005	.005	----	----	10.5
16507	B040	339.5	----	----	.005	.003	----	----	9.5
16517	B040	279.9	----	----	.004	.010	----	----	11.6

## REFERENCES

1. W. H. Appich, Jr. and R. E. Wittmeyer, "Copperhead Aerodynamic Test Data, Analyses, and Flight Simulation Model Development, Vol. I and II," Martin Marietta Corporation Report OR 15321, November 1978.
2. W. K. Rogers, Jr., "The Transonic Free Flight Range," Ballistic Research Laboratories Report Number 1044, Aberdeen Proving Ground, Maryland, June 1958. AD 200177.
3. E. R. Dickinson, "Physical Measurements of Projectiles," Technical Note 874, U. S. Army Ballistic Research Laboratories, Aberdeen Proving Ground, MD, February 1954, AD 803103.
4. C. H. Murphy, "Data Reduction for the Free Flight Spark Ranges," Report 900, U. S. Army Ballistic Research Laboratory, Aberdeen Proving Ground, MD, February 1954, AD 35833.
5. C. H. Murphy, "The Measurement of Non-Linear Forces and Moments by Means of Free Flight Tests," Report 974, U. S. Army Ballistic Research Laboratory, Aberdeen Proving Ground, MD, February 1956, AD 93521.

## APPENDIX

On 3 May 1979, the sixteenth round (B035 MOD) in the BRL XM712 test program was fired, at a test Mach number of approximately 1.75. A smear camera located roughly 3 metres in front of the muzzle brake showed that the plastic nose-cap had failed, and was disintegrating in flight. Figure A-1 is a photograph of the smear camera record.

The damaged projectile (Test Round No. 16520) entered the range, where it pitched upward, and continued to gain altitude until it impacted the steel roof trusses of the building, at the end of the third group of stations. Figures A-2 through A-6 are pitch-plane shadowgraphs showing the progress of Round 16520 through the first two groups of stations.

Figure A-2 shows the model at station 11, 19.8 metres from the gun, at an upward pitch angle of 4.5 degrees. The plastic nose-cap has completely broken off, and the fins are opening normally. At station 14, 38.2 metres out, the pitch angle has increased to 8.9 degrees, and is up to 10.1 degrees at station 15, 44.5 metres from the gun. By station 24, 83.7 metres out, the pitch angle has grown to 12.0 degrees, and has essentially reached a maximum of 12.1 degrees, at station 25, 90 metres out. The last data station before impact was station 35, 136 metres from the muzzle; the pitch angle at station 35 had decreased to 8.3 degrees. However, the large upward pitch angle had increased the flight-path climb angle from 0.46 degree at station 11 to 1.62 degrees at station 35, and the projectile had gained 1.95 metres in altitude over 96 metres of flight.

Surprisingly, a fairly good data reduction was obtained for Round 16520, and the results are given below:

Mach Number	$\bar{\alpha}_t$ (deg)	$C_D$	$C_{M_\alpha}$	$C_{N_\alpha}$	$C_{P_N}$ (cal.-base)
1.76	20.3	1.58	-0.67	8.10	3.63

The above results show that the broken nose-cap increases drag by roughly 120% over that of a normal XM712 projectile, at Mach number 1.76.

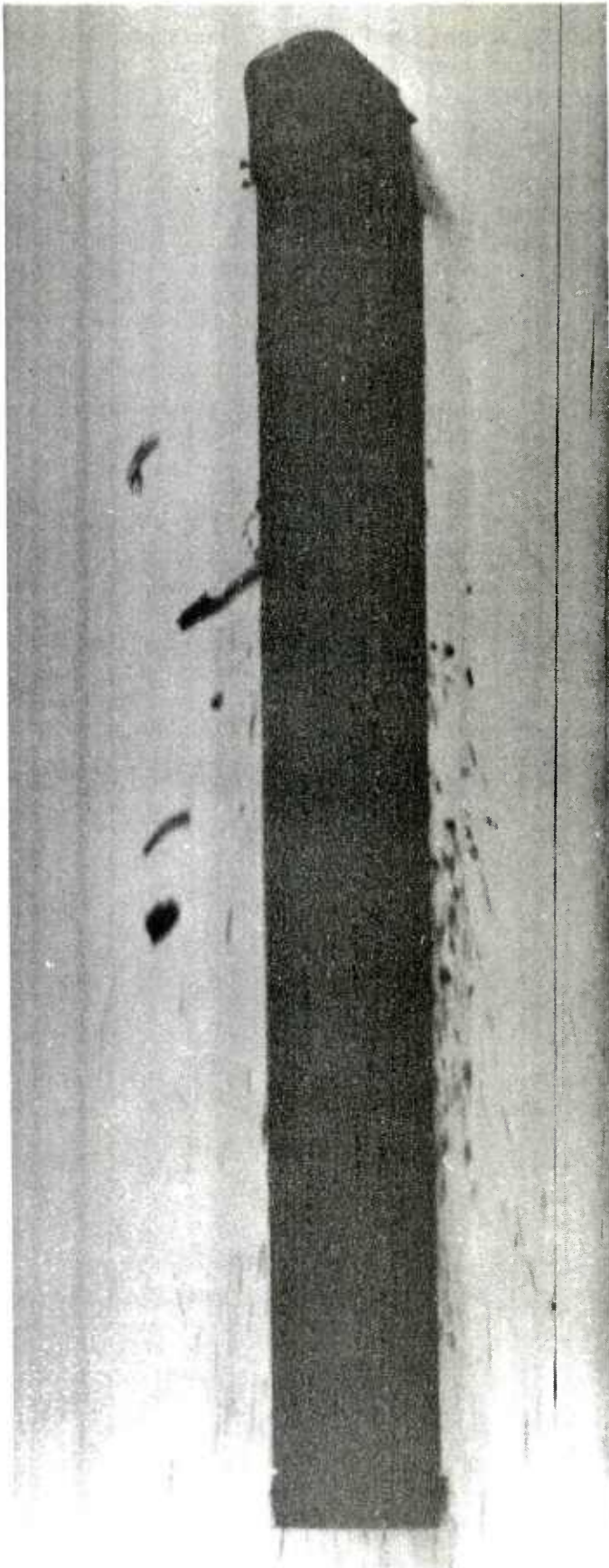


Figure A-1. Smear Camera Photograph of B035 MOD Model with  
Broken Nose Cap, Round No. 16520

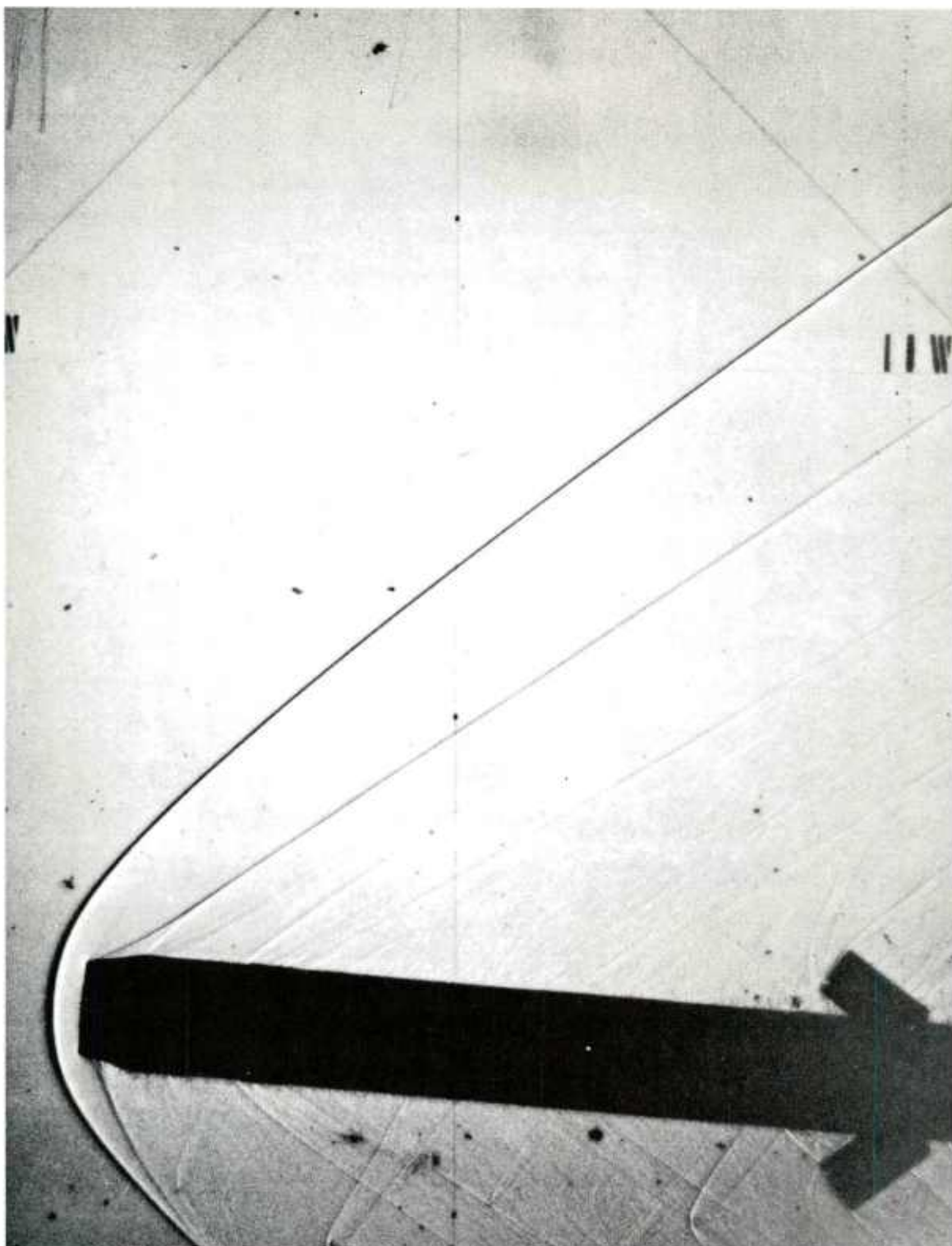


Figure A-2. Pitch-Plane Shadowgraph of Round No. 16520, Station 11

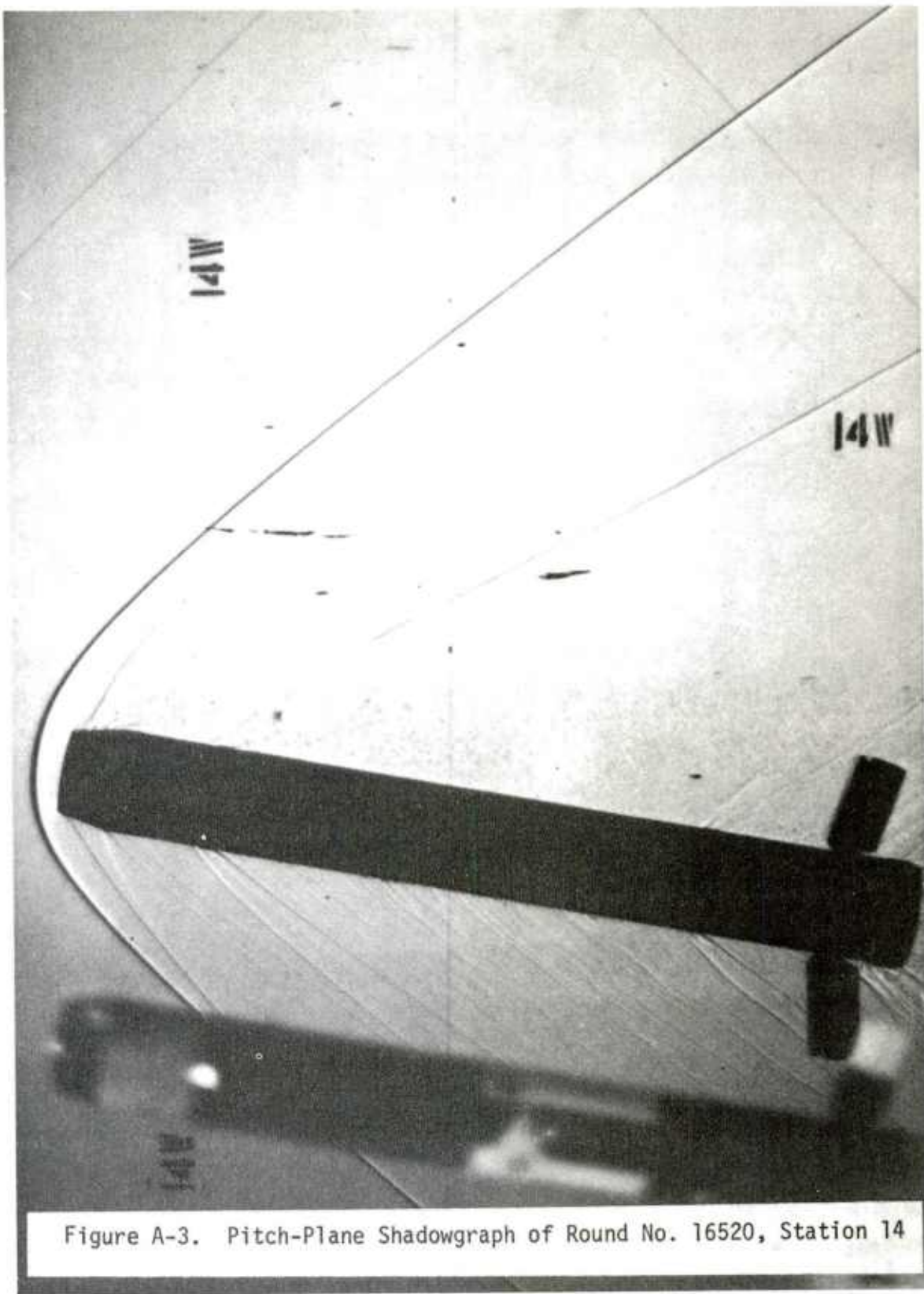


Figure A-3. Pitch-Plane Shadowgraph of Round No. 16520, Station 14

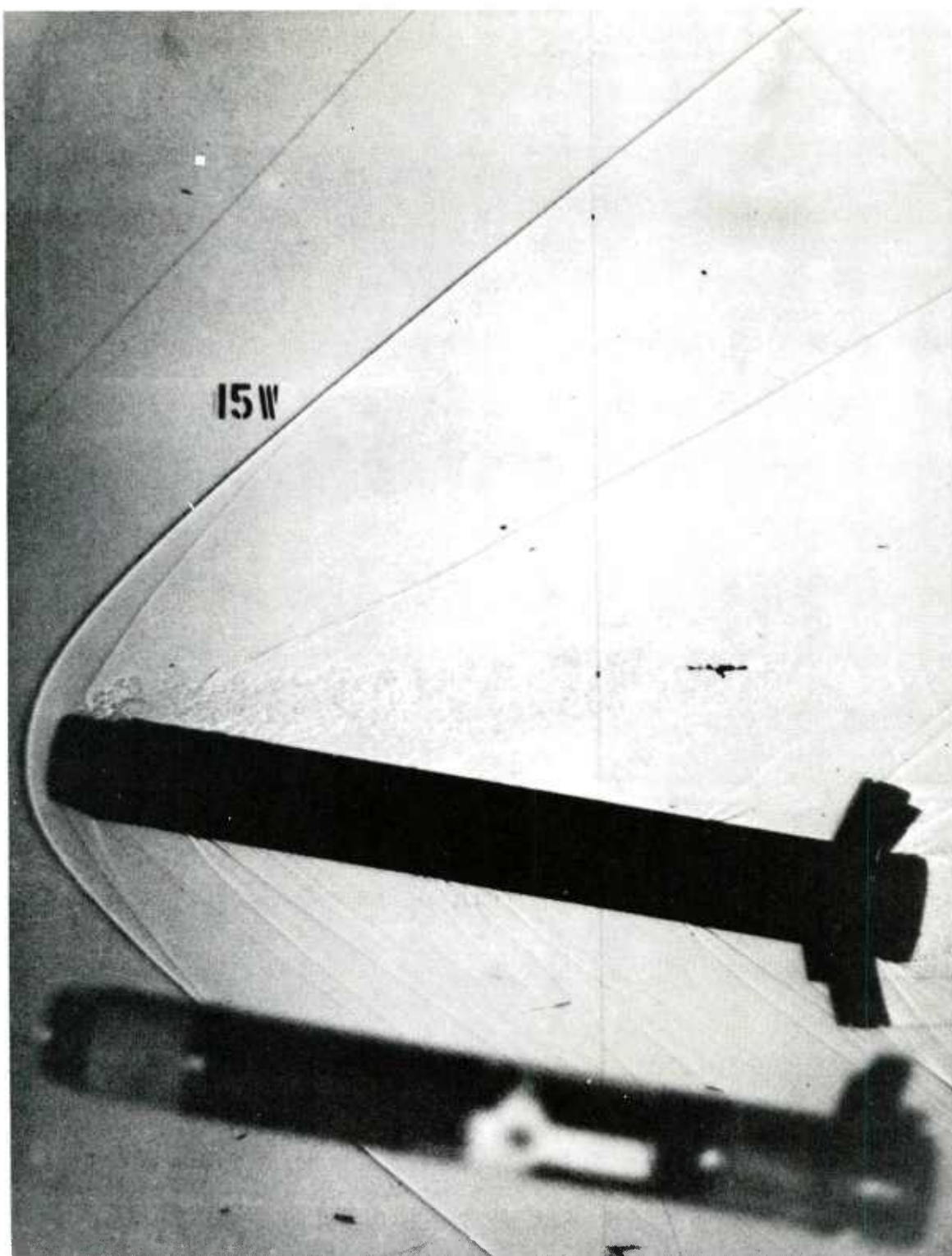


Figure A-4. Pitch Plane Shadowgraph of Round No. 16520, Station 15

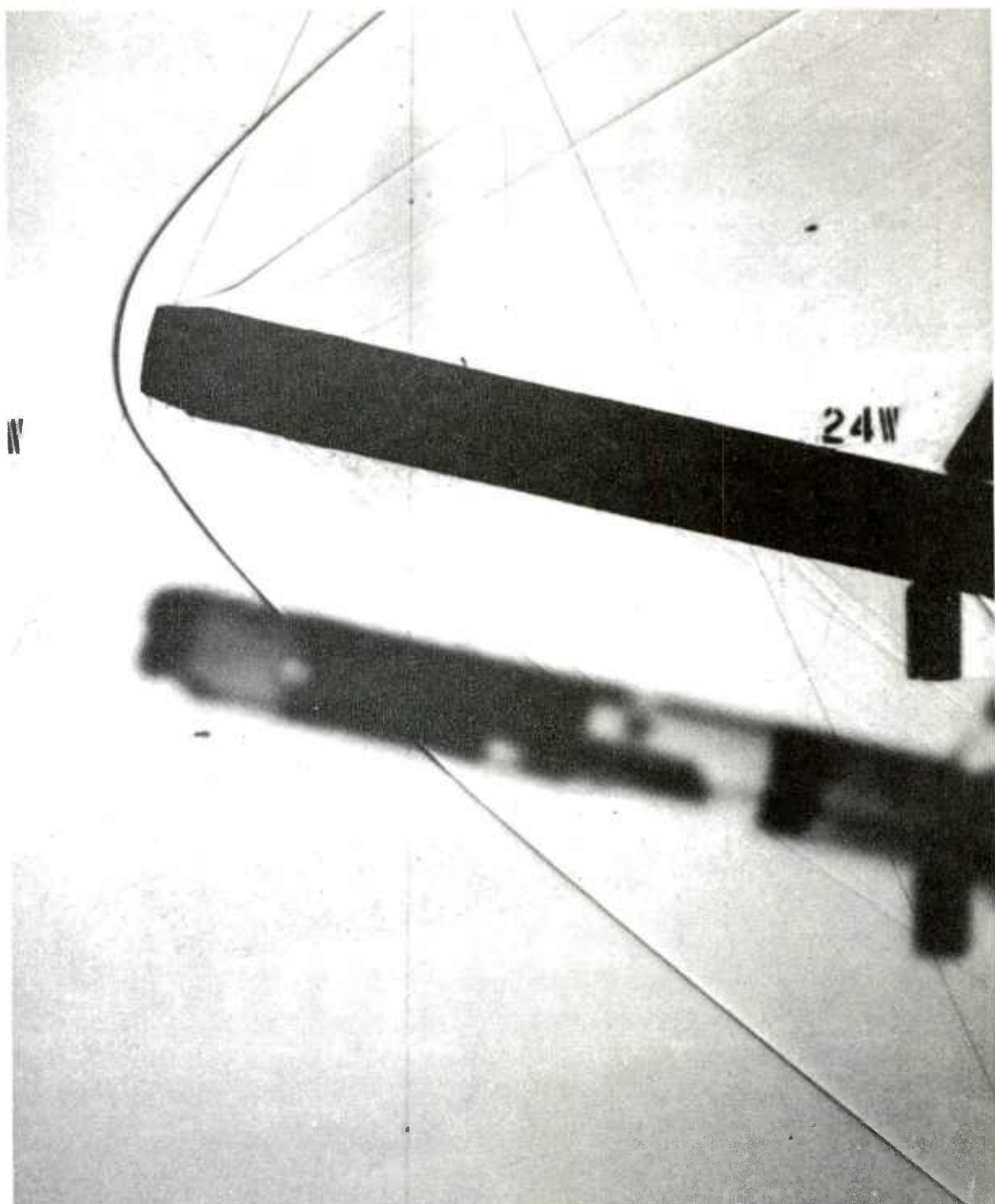


Figure A-5. Pitch Plane Shadowgraph of Round No. 16520, Station 24

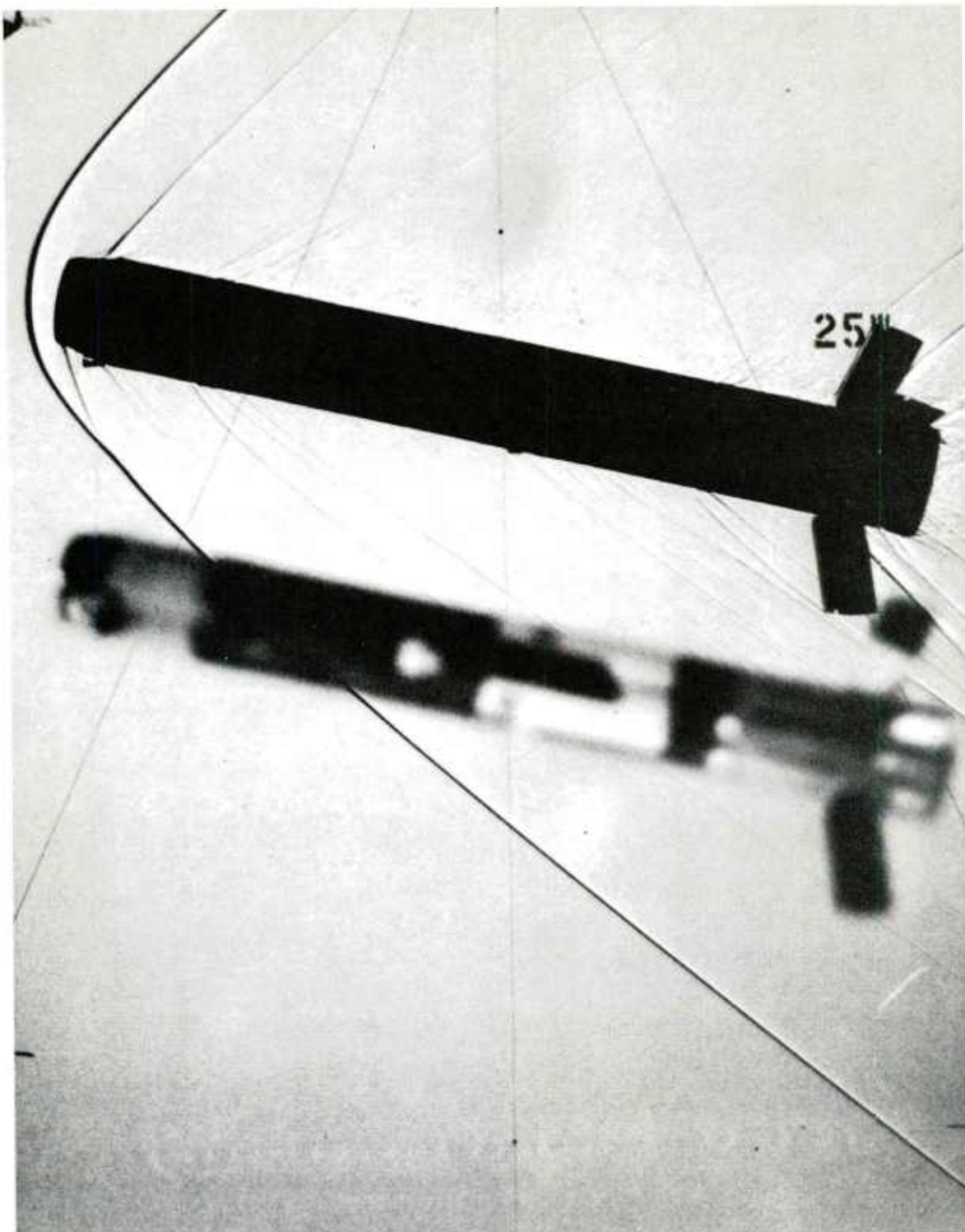


Figure A-6. Pitch Plane Shadowgraph of Round No. 16520, Station 25

LIST OF SYMBOLS

$C_D$	=	<u>Drag Force</u> $(1/2) \rho V^2 S$	
$C_{D_0}$	=	zero yaw drag coefficient	
$C_{D_{\delta^2}}$	=	yaw drag coefficient	
$C_{L_\alpha}$	=	<u>Lift Force</u> $(1/2) \rho V^2 S \delta$	Positive coefficient: Force in plane of total angle of attack, $\alpha_t$ $\perp$ to trajectory in direction of $\alpha_t$ . ( $\alpha_t$ directed from trajectory to missile axis.) $\delta = \sin \alpha_t$ .
$C_{N_\alpha}$	=	<u>Normal Force</u> $(1/2) \rho V^2 S \delta$	Positive coefficient: Force in plane of total angle of attack, $\alpha_t$ , $\perp$ to missile axis in direction of $\alpha_t$ . $C_{N_\alpha} \cong C_{L_\alpha} + C_D$
$C_{M_\alpha}$	=	<u>Static Moment</u> $(1/2) \rho V^2 S d \delta$	Positive coefficient: Moment increases angle of attack $\alpha_t$ .
$C_{M_{p\alpha}}$	=	<u>Magnus Moment</u> $(1/2) \rho V^2 S d \frac{pd}{V} \delta$	Positive coefficient: Moment rotates nose $\perp$ to plane of $\alpha_t$ in direction of spin.
$C_{N_{p\alpha}}$	=	<u>Magnus Force</u> $(1/2 \rho V^2 S \frac{pd}{V} \delta$	Negative coefficient: Force acts in direction of $90^\circ$ rotation of the positive lift force against spin.

For most exterior ballistic uses, where  $\dot{\alpha} = q$ ,  $\dot{\beta} = -r$ , the definition of the damping moment sum is equivalent to:

$$C_{M_q} + C_{M_{\dot{\alpha}}} = \frac{\text{Damping Moment}}{(1/2) \rho V^2 S d \frac{q_t d}{V}}$$

Positive coefficient: Moment increases angular velocity.

LIST OF SYMBOLS (continued)

$c_{\ell_p}$	$= \frac{\text{Roll Damping Moment}}{(1/2 \rho V^2 S d \frac{pd}{V})}$ Negative coefficient: Moment decreases rotational velocity.
$CP_N$	= center of pressure of the normal force, positive from base to nose.
$\alpha, \beta$	= angle of attack, side slip
$\alpha_t$	$= (\dot{\alpha}^2 + \beta^2)^{1/2} = \sin^{-1} \delta$ , total angle of attack
$\lambda_F$	= fast mode damping rate negative $\lambda$ indicates damping
$\lambda_S$	= slow mode damping rate
$\rho$	= air density
c.m.	= center of mass
$d$	= body diameter of projectile, reference length
$I_x$	= axial moment of inertia
$I_y$	= transverse moment of inertia
$K_F$	= magnitude of the fast yaw mode
$K_S$	= magnitude of the slow yaw mode
$m$	= mass of projectile
$\ell$	= length of projectile
$M$	= Mach number
$p$	= roll rate
$q, r$	= transverse angular velocities
$q_t$	$= (q^2 + r^2)^{1/2}$
$R$	= subscript denotes range value
$S$	$= \frac{\pi d^2}{4}$ , reference area
$s_g$	= gyroscopic stability factor
$V$	= velocity of projectile

DISTRIBUTION LIST

<u>No. of Copies</u>	<u>Organization</u>	<u>No. of Copies</u>	<u>Organization</u>
12	Commander Defense Technical Info Center ATTN: DDC-DDA Cameron Station Alexandria, VA 22314	3	Commander US Army Armament Research and Development Command ATTN: DRCPM-CAWS-GP Mr. E. Zimpo Mr. E. Manley Mr. H. Nobie Dover, NJ 07801
1	Commander US Army Materiel Development and Readiness Command ATTN: DRCDMD-ST 5001 Eisenhower Avenue Alexandria, VA 22333	2	Commander US Army Armament Research and Development Command ATTN: DRDAR-SCA-SC COL M. G. Swindler DRDAR-SC Mr. E. Malatesta Dover, NJ 07801
2	Commander US Army Armament Research and Development Command ATTN: DRDAR-TSS Dover, NJ 07801	1	Commander US Army Armament Readiness Command ATTN: DRSAR-LEP-L, Tech Lib Rock Island, IL 61299
11	Commander US Army Armament Research and Development Command ATTN: DRDAR-LCA-F Mr. A. Loeb DRDAR-LCA-FA Mr. S. Wasserman Mr. D. Mertz DRDAR-LCA-FB Mr. R. Kline Mr. E. Falkowski Mr. S. Kahn Mr. H. Hudgins Mr. E. Friedman Mr. C. Ng DRDAR-LCA Mr. W. R. Benson DRDAR-LCV Mr. R. Reisman Dover, NJ 07801	1	Director US Army Armament Research and Development Command Benet Weapons Laboratory ATTN: DRDAR-LCB-TL Watervliet, NY 12189
		1	Commander US Army Aviation Research and Development Command ATTN: DRSAV-E P.O. Box 209 St. Louis, MO 63166
		1	Director US Army Air Mobility Research and Development Laboratory Ames Research Center Moffett Field, CA 94035

## DISTRIBUTION LIST

<u>No. of Copies</u>	<u>Organization</u>	<u>No. of Copies</u>	<u>Organization</u>
1	Commander US Army Communications Rsch and Development Command ATTN: DRDCO-PPA-SA Fort Monmouth, NJ 07703	1	Commander US Army Research Office ATTN: CRD-MA-EII P. O. Box 12211 Research Triangle Park NC 27709
1	Commander US Army Electronic Research and Development Command Technical Support Activity ATTN: DELSD-L Fort Monmouth, NJ 07703	1	Commander US Army Standardization Group, UK Box 65 FPO New York 09510
1	Commander US Army Missile Command ATTN: DRSMI-R Redstone Arsenal, AL 35809	2	Chief US Army Standardization Group ATTN: DAMA-PPI, COL Noce National Defense Headquarters Ottawa, Ontario, Canada KIA OK2
1	Commander US Army Missile Command ATTN: DRSMI-YDL Redstone Arsenal, AL 35809	3	Chief US Army Standardization Group Australia San Francisco, CA APO 96404
1	Commander US Army Missile Command ATTN: DRSMI-RDK Mr. R. A. Deep Redstone Arsenal, AL 35809	1	Director US Army TRADOC Systems Analysis Activity ATTN: ATAA-SL, Tech Lib White Sands Missile Range NM 88002
1	Commander US Army Missile Command ATTN: DRSMI-RDK Mr. W.D. Washington Redstone Arsenal, AL 35809	1	Commander Naval Air Systems Command ATTN: AIR-604 Washington, DC 20360
1	Commander US Army Tank Automotive Research & Development Cmd ATTN: DRDTA-UL Warren, MI 48090	3	Commander Naval Ordnance Systems Command ATTN: ORD-0632 ORD-035 ORD-5524 Washington, DC 20360
1	Commander US Army Yuma Proving Ground ATTN: STEYP-TMW, W.T.Vomocil Yuma, AZ 85364		

DISTRIBUTION LIST

<u>No. of Copies</u>	<u>Organization</u>	<u>No. of Copies</u>	<u>Organization</u>
1	Commander Naval Air Development Center Johnsville Warminster, PA 18974	4	AFATL/DLDL (Dr. D. C. Daniel; Mr. K. Cobb; Mr. G. Winchenbach; Mr. K. West) Eglin AFB, FL 32542
1	Commander David W. Taylor Naval Ship Research & Development Ctr ATTN: Aerodynamics Laboratory Bethesda, MD 20084	2	APGC/PGTRI (Mr. C. Butler; Mr. E. Sears) Eglin AFB, FL 32542
5	Commander Naval Surface Weapons Center ATTN: Dr. Thomas Clare Dr. W. R. Chadwick Dr. W. G. Soper Dr. F. Moore Dr. T. R. Pepitone Dahlgren, VA 22448	4	Director Sandia Laboratories ATTN: Div 1342, W.F.Hartman Div 1331, H.R. Vaughn A. E. Hodapp W. Curry Albuquerque, NM 87115
1	Commander Naval Surface Weapons Center ATTN: Code 730, Tech Lib Silver Spring, MD 20910	4	Director National Aeronautics and Space Administration Ames Research Center ATTN: Dr. Gary Chapman Mr. A. Seiff Mr. Murray Tobak Tech Lib Moffett Field, CA 94035
1	Commander Naval Weapons Center ATTN: Code 233 China Lake, CA 93555	1	Director National Aeronautics and Space Administration George C. Marshall Space Flight Center ATTN: MS-I, Library Huntsville, AL 35812
1	Commander Naval Research Laboratory ATTN: Tech Info Div Washington, DC 20375	1	Director National Aeronautics and Space Administration Langley Research Center ATTN: MS 185, Tech Lib Langley Station Hampton, VA 23365
1	Superintendent Naval Postgraduate School Monterey, CA 93940		
1	AFATL (Tech Lib) Eglin AFB, FL 32542		

DISTRIBUTION LIST

<u>No. of Copies</u>	<u>Organization</u>	<u>No. of Copies</u>	<u>Organization</u>
1	Director National Aeronautics and Space Administration Lewis Research Center ATTN: Tech Lib 21000 Brookpark Road Cleveland, OH 44135	1	General Electric Company Armament Systems Department ATTN: Mr. Robert H. Whyte Lakeside Avenue Burlington, VT 05401
1	Director National Aeronautics and Space Administration Scientific and Technical Information Facility P. O. Box 8757 Baltimore/Washington International Airport MD 21240	1	Honeywell, Inc. Government & Aerospace Products Division ATTN: Mail Station MN 112190 G. Stilley 600 Second Street, N. Hopkins, MN 55343
1	Aerospace Corporation ATTN: Dr. Daniel Platus 2350E El Segundo Avenue El Segundo, CA 90245	2	Hughes Helicopter ATTN: Mr. R. Land Mr. B. Lindner Centinella and Teale Streets Culver City, CA 90230
1	Alpha Research, Inc. ATTN: Mr. J. E. Brunk P. O. Box U Santa Barbara, CA 93102	2	Martin Marietta Aerospace Orlando Division ATTN: MP-334 Mr. P. Morrison Mr. W. Appich Orlando, FL 32805
1	Calspan Corporation P. O. Box 400 Buffalo, NY 14221	3	Nielsen Engineering and Research, Incorporated ATTN: Dr. J. N. Nielsen Dr. J. R. Spreiter Dr. S. S. Stahara Mountain View, CA 94043
1	Chrysler Corporation Defense Division ATTN: Dr. R. Lusardi Detroit, MI 48231	1	Director Applied Physics Laboratory The Johns Hopkins University Johns Hopkins Road Laurel, MD 20810
1	General Dynamics Corporation ATTN: Electro-Dynamics Div Dr. D. L. Trulin P. O. Box 2507 Pomona, CA 91766	1	University of Delaware ATTN: Dept of Mechanical and Aerospace Eng., Dr. J. Danberg Newark, DE 19711

DISTRIBUTION LIST

<u>No. of</u>	<u>Copies</u>	<u>Organization</u>
1		University of Maryland ATTN: Mathematics Dept Prof. Y.M. Lynn 5401 Wilkins Avenue Baltimore, MD 21228
1		University of Notre Dame ATTN: Dept Aerospace Eng. Dr. T. J. Mueller South Bend, IN 46556
1		University of Virginia Department of Engineering Science and Systems ATTN: Prof. Ira D. Jacobson Thornton Hall Charlottesville, VA 22904

Aberdeen Proving Ground

Dir, USAMSAA  
ATTN: DRXSY-D  
DRXSY-MP, H. Cohen  
Cdr, USATECOM  
ATTN: DRSTE-TO-F  
Dir, USACSL, Bldg. E3516  
ATTN: DRDAR-CLB-PA

USER EVALUATION OF REPORT

Please take a few minutes to answer the questions below; tear out this sheet, fold as indicated, staple or tape closed, and place in the mail. Your comments will provide us with information for improving future reports.

1. BRL Report Number \_\_\_\_\_

2. Does this report satisfy a need? (Comment on purpose, related project, or other area of interest for which report will be used.)  
\_\_\_\_\_  
\_\_\_\_\_  
\_\_\_\_\_

3. How, specifically, is the report being used? (Information source, design data or procedure, management procedure, source of ideas, etc.)  
\_\_\_\_\_  
\_\_\_\_\_  
\_\_\_\_\_

4. Has the information in this report led to any quantitative savings as far as man-hours/contract dollars saved, operating costs avoided, efficiencies achieved, etc.? If so, please elaborate.  
\_\_\_\_\_  
\_\_\_\_\_  
\_\_\_\_\_

5. General Comments (Indicate what you think should be changed to make this report and future reports of this type more responsive to your needs, more usable, improve readability, etc.)  
\_\_\_\_\_  
\_\_\_\_\_  
\_\_\_\_\_

6. If you would like to be contacted by the personnel who prepared this report to raise specific questions or discuss the topic, please fill in the following information.

Name: \_\_\_\_\_

Telephone Number: \_\_\_\_\_

Organization Address: \_\_\_\_\_  
\_\_\_\_\_  
\_\_\_\_\_